polysaccharides

MDPI

Article

The Development of Thermoresponsive Multifunctional Chitosan Films Suitable for Food Packaging

Nihal Sarier [1,*], Anıl Eloglu [1] and Emel Onder [2,*]

[1] Faculty of Engineering, Istanbul Kultur University, Istanbul 34000, Turkey
[2] Faculty of Textile Technologies and Design, Istanbul Technical University, Istanbul 34000, Turkey
* Correspondence: n.sarier@iku.edu.tr (N.S.); onderem@itu.edu.tr (E.O.)

Abstract: We developed bio-based chitosan–gelatin films, CHG-LO films, incorporating lavender essential oil (15–26 wt% LO) and oleic acid (33–47 wt% OA) with smooth surfaces and thicknesses of 0.42–0.99 mm. For their manufacture, the nanoemulsions were prepared to possess uniform dispersion and colloidal stability with average droplet sizes of 475–854 nm, polydispersity indices (PDI) of 0.095–0.235, and zeta potentials of 23.7–56.9 mV at 40 °C, where OA served as surfactant and phase change material. The opacities of the CHG-LO films increased by 1.8 to 5.5 times compared to the control group, and their UV-visible light-blocking properties improved. These films demonstrated cyclic thermal buffering character, with heat storage capacities ranging from 14.0 to 36.0 $J \cdot g^{-1}$ between −26 °C and 20 °C compatible with that of OA. Additionally, they showed reduced water vapor transmission rates and swelling degrees in acidic and neutral environments. The total phenolic contents of the CHG-LO films increased 1.5–4.2 times compared to the control associated with the presence of LO phenolic groups in the structure. DPPH (2,2-diphenyl-1 picrylhydrazyl) and ABTS (2,2′–azino–bis(3–ethylbenzothiazoline–6–sulphonic acid)) scavenging activity test results show that the antioxidant properties of these films improved with increasing LO-OA content up to 2.2 and 1.3 times the control, respectively, and also showed antimicrobial properties. The multifunctional CHG-LO films of this study are promising candidates for temperature-sensitive active packaging in food as well as in pharmaceutical and cosmetic industries.

Keywords: chitosan; gelatin; lavender oil; oleic acid; PCM; DSC; XRD; AFM; contact angle

Academic Editor: Gordon Morris

Received: 25 October 2024
Revised: 17 January 2025
Accepted: 25 February 2025
Published: 2 March 2025

Citation: Sarier, N.; Eloglu, A.; Onder, E. The Development of Thermoresponsive Multifunctional Chitosan Films Suitable for Food Packaging. *Polysaccharides* **2025**, *6*, 17. https://doi.org/10.3390/polysaccharides6010017

1. Introduction

Food packaging plays an important role in preserving and transporting food products while maintaining their flavor and quality. Research groups and leading companies are making great efforts to discover and develop new packaging materials that can extend the shelf life of food products, coupled with the growing consumer demand for high-quality, healthier, and safer products. The global food packaging market is expected to grow from USD 418.98 billion in 2024 to USD 763.40 billion by 2032 [1].

Active packaging film is a type of film that intentionally includes active ingredients to enhance the safety or sensory properties of the packaged food, potentially extending the food's shelf life and ensuring the quality of the food [2–4]. Recent studies related to active packaging include oxygen scavengers, carbon dioxide emitters/absorbents, moisture absorbers, ethylene absorbers, ethanol emitters, fragrance emitter/absorber systems, time–temperature indicators, and films containing antioxidant and antimicrobial agents [4–6].

Films made of biopolymers are becoming increasingly important in the preparation of multifunctional food packaging [7,8]. Chitosan (CH), which is a versatile polycationic

polysaccharide, has attracted the attention of researchers due to its nontoxicity, biodegradability, biocompatibility, intrinsic antimicrobial and antifungal properties, film-forming ability, abundance in nature, and low cost. Thus, it has an excellent potential to be used as food packaging material [9–12]. CH is classified as generally safe by the US Food and Drug Administration (FDA), confirming its safety as a material suitable for preserving natural foods [13]. Gelatin is an important hydrocolloid, rich in protein structure, obtained by the hydrolysis of collagen, and widely used as a food packaging material due to its excellent gel-forming ability, abundance, and low cost [9–12]. Recently, chitosan–gelatin-based films have been increasingly used as biocompatible, intrinsically antioxidant, and antimicrobial packaging films with good physical properties [9–12]. The development of chitosan–gelatin-based films with enhanced antioxidant and antimicrobial properties and the protection of food products from air, light, and temperature fluctuations is an open research area [13–15].

In several current studies on active film production, researchers have incorporated various essential oils, including cinnamon, thyme, clove, bergamot, ginger, turmeric, garlic, rosemary, mustard, lemon, and limonene, into bio-based polymer matrices to impart antioxidant and antimicrobial properties to the films [16–19]. Lavender essential oil (LO), extracted from the Lavandula plant, with the major constituents of linalool, linalyl acetate, camphor, and eucalyptol, has been recently employed as a bioactive component to improve the antioxidant and antimicrobial properties of bio-based packaging films [20–22]. Although LO is generally recognized as safe for its intended uses [23], it has dose-dependent cytotoxicity due to its major components linalyl acetate and linalool, and, therefore, it should be used in small concentrations for film formation applications [24,25]. The most commonly employed technique for incorporating essential oils (EOs) into active films is the formation of oil-in-water (O/W) emulsions, whereby the hydrophobic EOs are uniformly dispersed in the hydrophilic film-forming mixture. A limited number of studies have investigated the emulsification of essential oils (EOs) in some commercial surfactants, including Tween 80, Tween 85, and Span 20, before their incorporation into the film-forming base [26]. For instance, Sun et al. developed LO-gelatin films in an O/W system with Tween 80 as a surfactant and reported that the films' antioxidant and antimicrobial properties as well as their hydrophobicity, water vapor barrier, and UV absorbance properties were improved, making them suitable for use in food packaging [27].

Temperature fluctuations during storage and distribution lead to quality deterioration in temperature-sensitive food products [28]. There is a need for active packaging films with thermal buffering capabilities to regulate the temperature of the food product within desired limits and to increase its shelf life, safety, and quality. Maintaining a storage temperature below 8 °C is crucial in cold chain transportation to ensure product safety during its transition from the supplier's controlled environment to the customer's controlled environment [29–31]. Standard materials used for product packaging, like low-density polyethylene (LDPE) and polystyrene (PS), have limited thermal insulation capabilities and fail to control temperature fluctuations. Phase change materials (PCMs), which absorb and release large amounts of heat during solid–liquid phase transitions, can be utilized to improve the thermal buffering capacity of food packaging materials [32–34]. A limited number of studies have investigated the use of composites containing PCMs in packaging films. For instance, Perez-Masia et al. prepared polycaprolactone (PCL), polylactide (PLA), and polystyrene (PS) nanostructured fibers containing dodecane, dodecanol, and paraffin PCMs with phase transitions at −10 °C or 5 °C for thermal insulation applications [35,36]. Chalco-Sandoval et al. developed PS multilayer films coated with electrospun mats of PCL-paraffin wax with a melting temperature of 5 °C for the storage of refrigerated foods [37]. Taş and Ünal prepared halloysite nanotubes (HNTs) containing PEG400 and PEG600 and

then incorporated them into polyethylene (PE) films for use in food packaging applications between −17–26 °C [38]. Vahabi et al. prepared three-layer PE coextruded films containing a paraffin mixture with a phase change temperature of 9 °C [39]. Karim et al. produced zein nanofibers comprising tetradecane as PCM and cinnamaldehyde as an antioxidant and antibacterial agent for cold storage at about 4–10 °C [40].

Oleic acid (OA) is a monounsaturated fatty acid found in many vegetable oils, which has been recognized as a safe substance by the FDA (21 CFR 172.860) for direct addition to foods and use as a lubricant, binder, and anti-foaming agent in the manufacture of foods and other food-grade additives [41]. Recently, OA has attracted some attention as PCM due to its low melting temperature range (4–17 °C), very high latent heat, low supercooling tendency, small volume change during phase change, self-nucleation behavior, chemical stability, natural availability, biodegradability, diversity, and low cost [42,43]. However, research on the temperature regulation function of OA in food packaging applications is quite limited and new. Drago et al. produced electrospun PCL fibers by loading linoleic and oleic acid as natural PCMs for food packaging in a cold supply chain; however, they did not observe the characteristic melting peaks of linoleic acid and oleic acid at −10 °C and 4–8 °C in their products [44]. OA is also known for its excellent emulsifying properties, making it a suitable candidate for stable emulsion formulations. As it is liquid at room temperature, it is readily miscible with the biopolymer bases without further heating [45,46]. It has been reported that the presence of oleic acid with essential oils in film-forming blends improves the mechanical properties, resistance to water vapor permeability, and thermal stability of the films, as well as the discoloration caused by the essential oils [47–49]. OA also synergistically contributes to the antioxidant and antimicrobial properties of film blends [50].

To the best of our knowledge, previous research to date has not fully addressed the use of OA as both a surfactant and a PCM in bio-based films. Furthermore, the research on chitosan–gelatin-based films containing LO and OA together was not found. In the present study, we aimed to develop chitosan–gelatin-based films (CHG-LO films) incorporating varying levels of lavender essential oil and oleic acid, ranging from 15–26 wt% LO and 33–47 wt% OA, to investigate their potential use as temperature-sensitive active packaging films. In addition to the heat-storing capacity for thermal buffering, UV-visible light transmission and opacity, swelling, and solubility in water, water vapor transmission rates, antioxidant, and antimicrobial activities were analyzed to examine the multifunctionality of the developed CHG-LO films.

2. Materials and Methods

2.1. Materials

The materials used in film production are as follows. Chitosan ($[C_6H_{11}NO_4]_n$; Poly(D-glucosamine); CAS No: 9012-76-4; MW: 100,000–300,000 g·mol^{-1}) was obtained from ACROS Organics (Morris, NJ, USA). Gelatin (CAS 9000-70-8; from bovine skin, Type B, protein ratio 70–90%, gel strength 225 g Bloom; powder) and glycerin (analytical), acetic acid (analytical, CH_3COOH), ethanol (technical, C_2H_5OH) and $CaCl_2{\cdot}2H_2O$ (technical), and oleic acid (cis-9-Octadecenoic acid; CAS: 112-80-1; MW: 282.46 g·mol^{-1}; d = 0.89 g·cm^{-3}; HLB: 11.7, 90% purity) were all purchased from Merck KGaA (Darmstadt, Germany). Lavender essential oil (Lavandula Angustifolia Herb Oil; Lavender Oil) obtained by steam distillation of the lavender plant from the Mediterranean region was purchased from Arifoğlu Spice and Food Industry & Trade Ltd. (Istanbul, Turkey). The chemical structures of chitosan, gelatin, oleic acid, and lavender essential oil are given in Figure 1.

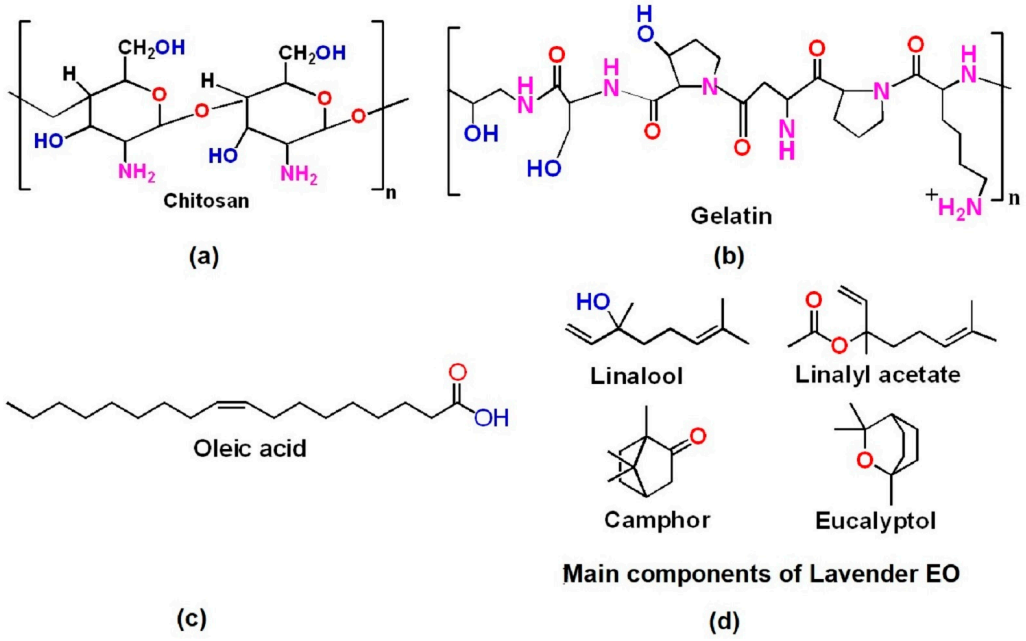

Figure 1. Chemical structure of (**a**) chitosan; (**b**) gelatin (adapted from [51]); (**c**) oleic acid; (**d**) lavender essential oil (adapted from [52]).

2.2. Preparation of the CHG Film Samples

Chitosan dissolves easily in acidic aqueous solutions with a pH not exceeding 6.3, due to the protonation of amine groups (-NH_2) at the 2nd carbon (C2) of glucosamine monomer [10]. To prepare a 2.0 wt% chitosan [CH (aq)] solution, 10.0 g of chitosan was stirred in 500.0 mL of 1.0 wt% (0.17 M) acetic acid (aq) solution for 8 h at 1500 rpm in a water bath at 75 °C. Next, a 10.0 wt% solution of gelatin [GE (aq)] was prepared by adding 100.0 g of gelatin to 500.0 mL of distilled water, then mixed in a water bath at 75 °C at 300 rpm for 120 min. Then, all of the solutions were stored in sealed containers.

For the emulsification of LO in the aqueous mixture of chitosan and gelatin, 1.0–2.0 mL of LO was thoroughly mixed with 1.0–4.5 mL of OA initially with an ultrathorax apparatus (Vortex Genius 3, IKA-Werke GmbH & Co. KG, Staufen, Germany) at 5500 rpm for 5 min. Then, 53.5 mL of 2.0 wt% CH (aq), 10.7 mL of 10.0 wt% GE (aq), and 0.5 mL glycerol were added to a beaker at 70 °C and mixed at 5500 rpm for 60 s. Subsequently, the organogel of LO and OA was added in a dropwise manner while maintaining stirring, followed by the addition of 1.0 mL of 5.0 wt% $CaCl_2$ (aq) for 120 s at a pH between 4.01 and 4.30 to facilitate the formation of chitosan and gelatin complexes and prevent chitosan precipitation in the solution [33]. Next, nanoemulsions were formed by ultrasonication at 50 kHz, 500 W, and 70–80% amplitude with a pulse rate of 5.5:0.0 for 30 min at 40 °C (CY-500 model Selecta Optic Ivymen System, Ultrasonic Homogenizer, J.P. Selecta, Barcelona, Spain). Table 1 displays the compositions of CHG nanoemulsions. Characterization methods of the CHG nanoemulsions are summarized in Supporting Information S1 [53].

Table 1. The nanoemulsion compositions used in the manufacture of CHG films (GE: gelatin; CH: chitosan; LO: lavender essential oil; oleic acid: OA).

Nanoemulsions of CHG Films	GE (aq) 10.0 wt% (mL)	CH (aq) 2.0 wt% (mL)	$CaCl_2$ (aq) 5.0 wt% (mL)	Glycerol (mL)	LO		OA	
					V (mL)	Wt%	V (mL)	Wt%
CHG	10.7	53.5	1.00	0.50	0.00	0.00	0.00	0.00
CHG-LO13	10.7	53.5	1.00	0.50	1.00	15.0	2.50	38.0
CHG-LO20	10.7	53.5	1.00	0.50	2.00	38.0	0.00	0.00
CHG-LO23	10.7	53.5	1.00	0.50	2.00	26.0	2.50	33.0
CHG-LO24	10.7	53.5	1.00	0.50	2.00	23.0	3.50	41.0
CHG-LO25	10.7	53.5	1.00	0.50	2.00	21.0	4.50	47.0

The CHG nanoemulsions were poured into plastic Petri dishes (2R = 11.5 cm) and left to solidify and dry for seven days in a well-ventilated environment at 18 °C. The pre-dried samples were then placed in an oven at 40 °C for the next seven days. The mass and thickness values of the dried CHG film samples were obtained as given in Supporting Information S2.

2.3. Characterization of the CHG Films

2.3.1. Structural and Surface Characterizations

Fourier transform infrared (FT-IR) transmission spectra of the films were recorded between 4000−650 cm^{-1} at a resolution of 4 cm^{-1} using a Perkin Elmer Spectrum 100 FTIR Spectrometer (PerkinElmer Life and Analytical Sci., Shelton, CT, USA) equipped with a universal attenuated total reflection (ATR) accessory. Wide-angle X-ray diffraction (WAXD) measurements of the films were carried out at room temperature using a D/MAX-YA diffraction meter (Rigaku Co., Tokyo, Japan) with a 100 mA CuKα tube. Diffraction patterns were determined in the 2θ = 3.00–40.00° diffraction angle range. The surface morphologies were determined by both scanning electron microscope (SEM) and atomic force microscope (AFM) analyses. The SEM images were taken by EVO® LS 10 model Zeiss type SEM (Jena, Germany) under an acceleration voltage of 10.00 kV. The 2D and 3D images of the films were scanned for 10 × 10 μm^2, 20 × 20 μm^2, and 40 × 40 μm^2 areas by NT-MDT NTEGRA Solaris model Atomic Force Microscope (NT-MDT, Zelenograd, Russia) in semicontact mode at 5 $\mu m \cdot s^{-1}$ scan speed, using an AppNano-NSG03 series Au-silicon cantilever (Tip curvature radius—less than 10 nm, resonant frequency: 90 kHz, Force constant—1.74 N/m).

2.3.2. Thermal Analyses

DSC analyses were performed using a Perkin Elmer DSC 4000 differential scanning calorimeter (Perkin Elmer Life and Analytical Sci., Waltham, MA, USA) with an accuracy of ±0.001. A nitrogen flux (20 $mL \cdot min^{-1}$) was used as the purge gas for the furnace. The films to be analyzed were primarily dried at 40 °C and stored in a desiccator. Approximately 10.0 mg test specimen of each film was scanned in the range of −45 to 45 °C at 10 $°C \cdot min^{-1}$ through 10 successive cycles. The thermogravimetric (TG) analyses were carried out from room temperature to 600 °C at 10 $°C \cdot min^{-1}$ heating rate under a dry nitrogen atmosphere purged at a flow rate of 150 $mL \cdot min^{-1}$ by a SEIKO EXSTAR 6200 Model TG/DTA instrument (Seiko Instrument Inc., Chiba, Japan).

2.3.3. Optical Properties

The optical properties of the CHG film samples were determined via color measurements and UV-visible light transmittance measurements [54] as given in Supporting Information S3.

2.3.4. pH-Dependent Swelling Degree, Water Solubility, and Water Vapor Transmission Rate Measurements

The pH-dependent swelling behavior and solubility of the CHG film samples were examined using buffer solutions of pH 3.0 and 7.0 in line with the literature [55]. The detailed methods are given in Supporting Information S4. Water vapor transmission tests were performed at 20 °C based on ASTM E96-00 (2005) with some modifications [56]. The details of the method are presented in Supporting Information S5.

2.3.5. The Contact Angle Measurements

Static contact angle measurements were carried out on the contact angle measuring instrument (Dataphysics OCA 50 Micro model, Dataphysics Instruments GmbH, Filderstadt, Germany) using the sessile drop technique [57]. Then, 4.5 µL of bidistilled water was dropped onto the film surface (2 cm × 10 cm) by micropipette at room temperature and the drop image was photographed subsequently with a high-speed video camera in 5 min. The contact angles of the droplets were calculated by image analysis software (Dataphysics SCA20_M4, Dataphysics Instruments GmbH, Filderstadt, Germany) using the Laplace–Young method. Three droplet images were obtained for each film surface.

2.3.6. Antioxidant and Antimicrobial Properties

The total phenolic content (TPC) of the films was determined using the Folin-Ciocalteu method [58], with some modifications. The antioxidant activity of the film samples was assessed spectrophotometrically using DPPH (2,2-diphenyl-1 picrylhydrazyl) [59] and ABTS (2,2′–azino–bis(3–ethylbenzothiazoline–6–sulphonic acid)) [60] free radical scavenging tests. The details of the methods are given in Supporting Information S6.

The antimicrobial activity of the films was determined by the standard methods applied for substances and materials in contact with food and the tests were carried out by an accredited food laboratory. These were the Detection and Counting of Total Coliform Bacteria (ISO 4832) [61], the Detection and Counting of Coagulase Positive Staphylococci (ISO 6888-1) [62], the Detection and Enumeration of Pseudomonas Aeruginosa (ISO 13720) [63], and the Search for Listeria 1 Monocytogenes (SWAP) according to ISO 11290-1 [64].

3. Results and Discussion

3.1. Characteristics of the CHG Nanoemulsions

Table 2 presents the density, pH, relative viscosity, and conductivity values of the CHG nanoemulsions.

Table 2. The physicochemical properties of CHG nanoemulsions.

Nanoemulsions of CHG Films	d ($g \cdot mL^{-1}$)	pH	Relative Viscosity $\eta_{relative}$	Conductivity (mS)	Z_{avg} (nm)	Polydispersity Index (PDI)	ζ-Potential (mV)
CHG	1.02	5.00	61.5	5.70	1726	0.354	11.9
CHG-LO13	1.01	3.87	18.0	3.73	475	0.235	53.3
CHG-LO20	1.00	4.09	18.8	3.60	492	0.101	46.9

Table 2. *Cont.*

Nanoemulsions of CHG Films	d ($g \cdot mL^{-1}$)	pH	Relative Viscosity $\eta_{relative}$	Conductivity (mS)	Z_{avg} (nm)	Polydispersity Index (PDI)	ζ-Potential (mV)
CHG-LO23	1.01	4.05	23.8	3.40	640	0.095	56.9
CHG-LO24	1.04	4.67	38.8	3.28	527	0.230	27.5
CHG-LO25	1.04	4.64	42.1	3.38	854	0.233	23.7

The relative viscosity values of the CHG-LO film-forming nanoemulsions decreased with the addition of both LO and OA compared to the CHG control nanoemulsion. In addition, the pH values of LO-OA micelle-loaded film-forming mixtures decreased to the range of 3.87–4.67 due to the acidity of OA compared to pH 5.00 of CHG control, which is suitable for chitosan–gelatin film formation [65]. The nanoemulsions containing LO-OA micelles exhibited lower conductivities, with values ranging from 3.28 to 3.89 mS relative to the conductivity of the CHG control nanoemulsion (5.70 mS). This can be attributed to the gradual immobilization of chitosan–gelatin chains around the LO-OA droplets, which improves the stability of the nanoemulsions, consistent with previous studies [66].

Accordingly, Table 2 also presents data on the average droplet size (Z_{avg}), polydispersity index (PDI), and zeta potential (ζ potential) for the CHG nanoemulsions at 40 °C. The CHG control presented the highest droplet size and PDI values and the lowest ζ-potential among all samples. The PDI values of 0.095–0.235 measured for CHG-LO nanoemulsions indicated good homogeneity of dispersions. Similar results were obtained by Xavier et al. [67] in the encapsulation of Cinnamodendron essential oil using zein as wall material. In CHG-LO nanoemulsions, the presence of LO-OA micelles resulted in an increase of the ζ-potential with a positive sign (+23.7 to +56.9 mV), indicating that chitosan and gelatin molecules were effectively adsorbed on the LO-OA nano droplet surfaces. Thus, the formation of highly charged positive particles caused repulsive forces, prevented flocculation, and provided enhanced colloidal stabilization [67]. Z_{avg} values for LO-OA-containing nanoemulsions were obtained between 475 and 854 nm, significantly lower than that of the CHG control nanoemulsion. A similar decreasing trend in droplet size was also observed by Sharma et al. in curcumin-loaded oil-in-water nanoemulsions prepared by ultrasonication using Tween 20 as a surfactant [68]. On the other hand, in CHG-LO23 (LO: 26 wt%, OA: 33 wt%), CHG-LO24 (LO: 23 wt%, OA: 41 wt%), CHG-LO25 (LO: 21 wt%, OA: 47 wt%) nanoemulsions, Z_{avg} values slightly increased compared to CHG-LO13 (LO: 15 wt%, OA: 38 wt%) due to higher amount of LO-OA micelles in the medium parallel to the literature [69].

3.2. Characteristics of the CHG Films

The film samples have smooth surfaces with a uniform yellowish appearance (See Figure 2).

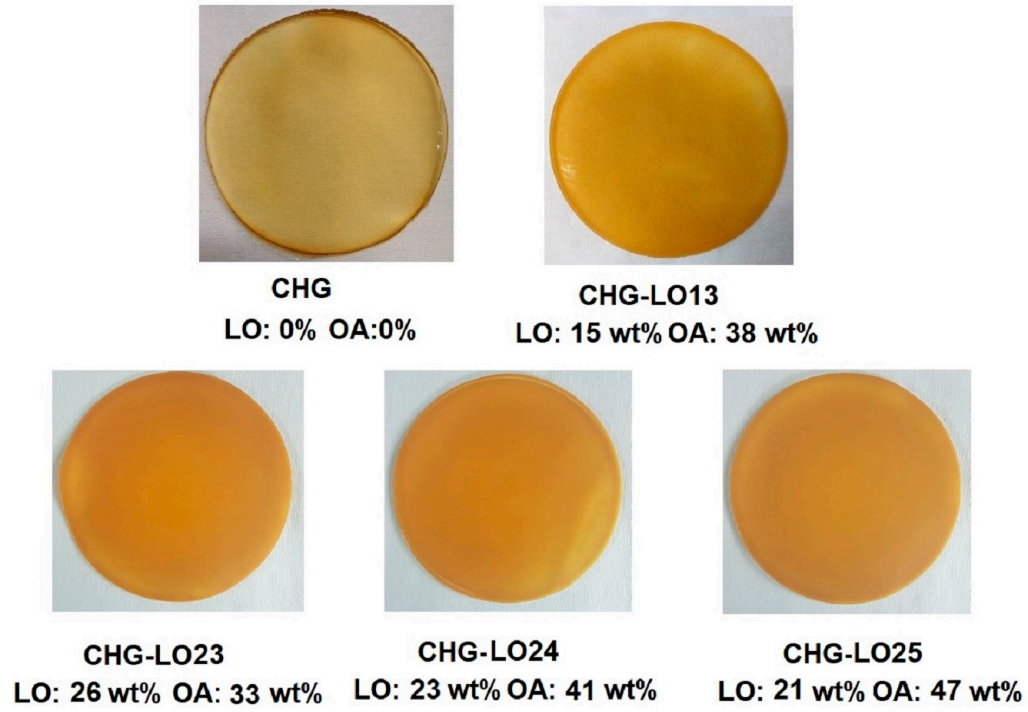

Figure 2. Images of the CHG film samples.

3.2.1. Optical Properties of the Films

Table 3 illustrates the surface color parameters (L*, a*, and b*), the total color difference (ΔE), and the opacity values of the CHG films. The L* values demonstrated a declining trend with the inclusion of LO and OA into the chitosan–gelatin matrix, while the values of a*, b*, and the total color difference (ΔE) gradually increased, which could be attributed to the characteristic light-yellow color of LO as well as that of OA [21,27]. The opacity of CHG film was obtained as 0.78 ± 0.01 mm^{-1}. The light scattering induced by LO-OA droplets resulted in notable increases in the opacity of CHG-LO films. These results coincide with those found by Sánchez-González et al. [69] and Moalla et al. [70] for chitosan-based composite films containing essential oils. In particular, the opacities of CHG-LO films lower than 5.0 are suitable to clearly show the packaging content and the condition of the food, as stated by Lei et al. [71].

Table 3. The surface color parameters (L*, a*, and b*), the total color difference (ΔE*), and the opacity values at 600 nm of the CHG films.

Specimen	L^*_{avg}	a^*_{avg}	b^*_{avg}	ΔE^*_{avg}	Opacity (mm^{-1})
CHG	73.60 ± 0.54	6.41 ± 1.25	48.9 ± 0.97	55.69 ± 1.23	0.78 ± 0.01
CHG-LO13	62.02 ± 0.38	12.75 ± 0.50	50.42 ± 0.76	62.70 ± 0.38	4.35 ± 0.02
CHG-LO20	58.58 ± 2.01	16.29 ± 0.88	52.57 ± 2.51	67.04 ± 0.89	3.01 ± 0.02
CHG-LO23	61.69 ± 0.11	13.79 ± 0.22	54.74 ± 0.23	66.79 ± 0.19	4.25 ± 0.16
CHG-LO24	67.21 ± 2.02	13.83 ± 0.15	52.38 ± 0.73	62.42 ± 0.11	1.41 ± 0.12
CHG-LO25	60.42 ± 1.12	13.33 ± 0.08	45.89 ± 0.58	59.82 ± 0.90	2.61 ± 0.09

As illustrated in Figure 3, the UV transmittance values in the range of 200–400 nm of all film samples decreased to 0.0–0.1% associated with UV absorbance characteristic of chitosan due to the existence of C=O double bonds and phenolic compounds of LO [72], suggesting that they are effective UV absorbers. The transparency of CHG-LO films in

the visible region between 400–800 nm exhibited a simultaneous decrease parallel to the increase in their opacity.

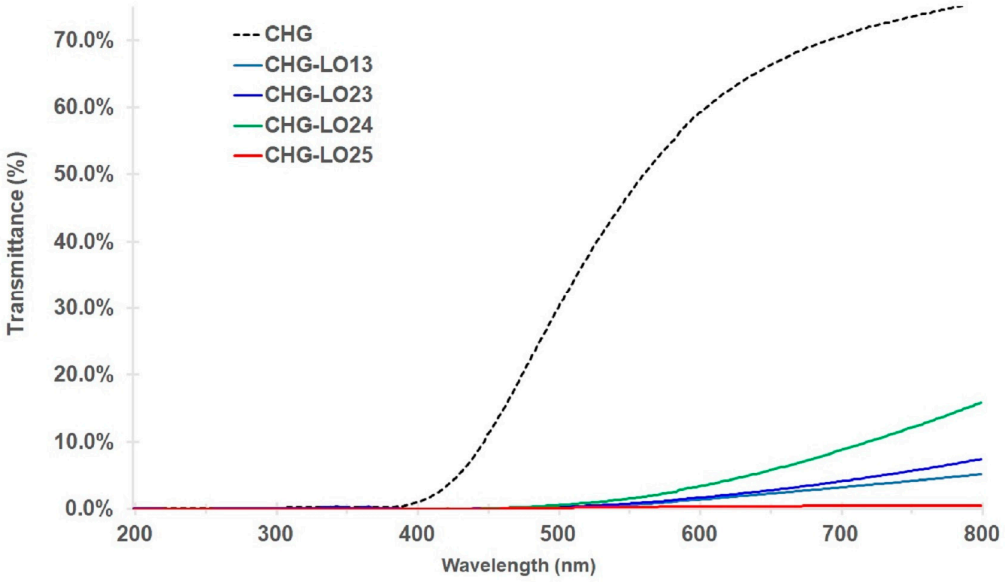

Figure 3. Transmittance (%) versus wavelength (nm) spectra of the CHG film samples in UV and visible regions.

3.2.2. Structural Characterizations of the CHG Films

Figure 4 shows the FTIR spectra of oleic acid (OA), lavender oil (LO), chitosan (CH), gelatin (GE), CHG control, and the CHG-LO films (the original FTIR spectra of all samples are given in Supporting Information S7).

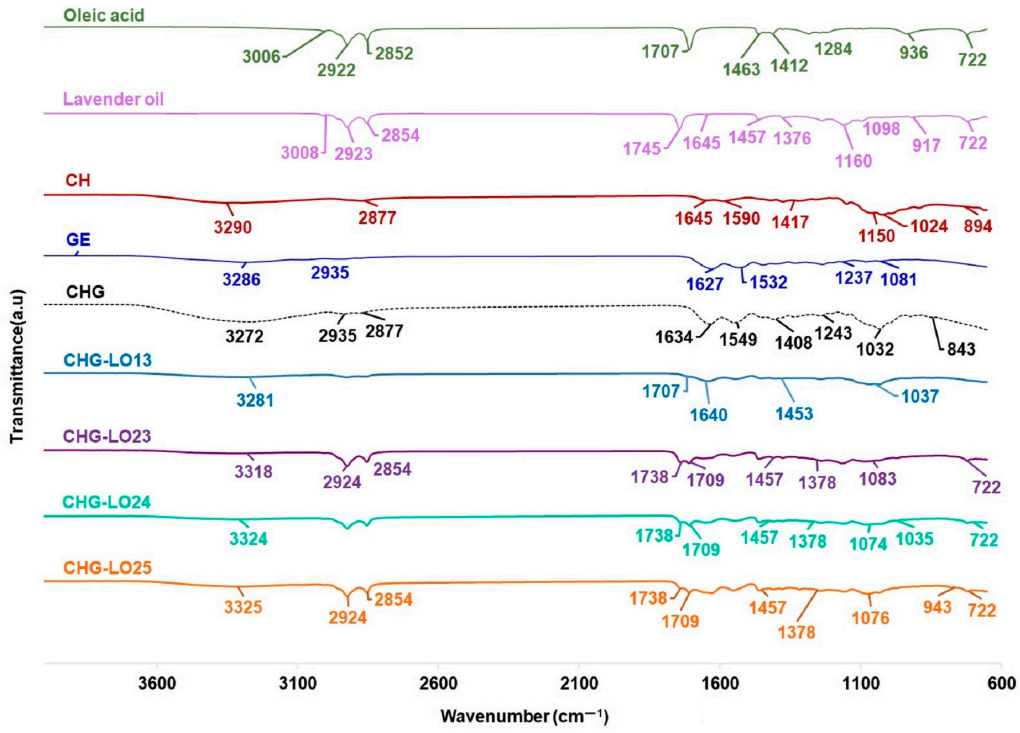

Figure 4. FTIR spectra of oleic acid (OA), lavender oil (LO), chitosan (CH), gelatin (GE), CHG control, and the CHG-LO films.

The large and broad CHG band observed at 3272 cm^{-1} belongs to the vibration of the –NH stretching, and –O−H groups of free water [73]. The CHG bands at 2935 cm^{-1} and 2877 cm^{-1} belong to the $-CH_2$ asymmetric and symmetric stretching vibrations and the band at 1408 cm^{-1} belongs to the $-CH_2$ bending vibrations of chitosan and gelatin, respectively. The 1634 cm^{-1} band is attributed to the −C=O and −OH stretching bands of chitosan and gelatin [73,74]. The bands at 1549 cm^{-1} and 1243 cm^{-1} are associated with the −NH bending and −CN stretching vibrations of chitosan and gelatin [74,75]. The bands observed at 1151 cm^{-1} and 1032 cm^{-1} are indicative of the characteristic C−O−C and −C=O stretching bands of chitosan [73,74]. The small bands observed in the range of 1000−800 cm^{-1} are attributed to the skeletal stretching of chitosan and gelatin [73].

The FTIR spectra of the CHG-LO films containing different ratios of LO and OA display the characteristic bands corresponding to the functional groups in the organic structures of chitosan, gelatin, LO, and OA in all samples with small shifts. For example, −NH and −OH stretching vibration bands of chitosan and gelatin are observed between 3325−3281 cm^{-1} in the IR spectra of CHG-LO films. The intense bands at 2924−2854 cm^{-1} are attributed to the stretching vibrations of $–CH_2$ groups of chitosan, gelatin, LO, and OA, while the bands at 1659−1630 cm^{-1} and 1242−1239 cm^{-1} are associated with their −C=O and −OH stretching vibrations [73–75]. The specific band of LO at 1745 cm^{-1} belonging to the stretching vibrations of carbonyl groups attached to the aromatic ring, and its band at 1376 cm^{-1} belonging to the stretching vibrations of phenolic –OH groups are observed at 1738 cm^{-1} and 1378 cm^{-1} in the FTIR spectrum of CHG-LO films, respectively [76]. The characteristic bands of LO at 1457 cm^{-1} induced by methylene −CH bending vibrations [20], and at 1160 cm^{-1} corresponding to C−O stretching are observed at 1457 cm^{-1} and 1163−1157 cm^{-1}, respectively, in the IR spectra of the CHG-LO films. The intense band at 1709 cm^{-1} is attributed to the asymmetric stretching of carbonyl groups (−C=O) and the band at 1284 cm^{-1} corresponds to the C−O stretching of the carbonyl groups of oleic acid [77,78]. The band at 722 cm^{-1} is induced by the rocking of methylene $–(CH_2)_n$ groups of lavender oil and oleic acid [76,78]. These results indicate that the chitosan–gelatin film formation and the incorporation of LO and OA micelles into their structures were accomplished.

Figure 5 shows XRD graphs of CHG control, CHG-LO13, CHG-LO23, CHG-LO24, and CHG-LO25. The XRD analysis of the CHG control reveals a diffraction peak at 8.4°, due to the presence of the triple helical structure of gelatin, and two peaks at 11.5° and 18.3° corresponding to the relatively ordered crystal lattice of chitosan [74]. The broader band at 2θ = 20.0–24.2° is attributed to the characteristic of the partially amorphous and partially crystalline chitosan–gelatin matrix [79]. In the XRD patterns of CHG-LO13, CHG-LO23, CHG-LO24, and CHG-LO25, intensities of the peaks at 8.4°, 11.5°, and 18.3° decreased significantly as a result of the integration of nanoscale LO-OA micelles into the chitosan–gelatin matrices. However, the intensities of the peaks at 20.0–24.2°, associated with the network structure formed between the chitosan–gelatin chains and LO-OA micelles, demonstrated an increase, accompanied by a reduction in peak width in comparison to the CHG control, indicating an improvement in the partial crystallinity of the film samples in these regions. Similar XRD findings were reported by Pérez-Córdoba et al. for gelatin-chitosan films incorporated with tocopherol/cinnamaldehyde and garlic oil [80]. And Rubilar et al. for chitosan films with carvacrol and grape seed extract [81].

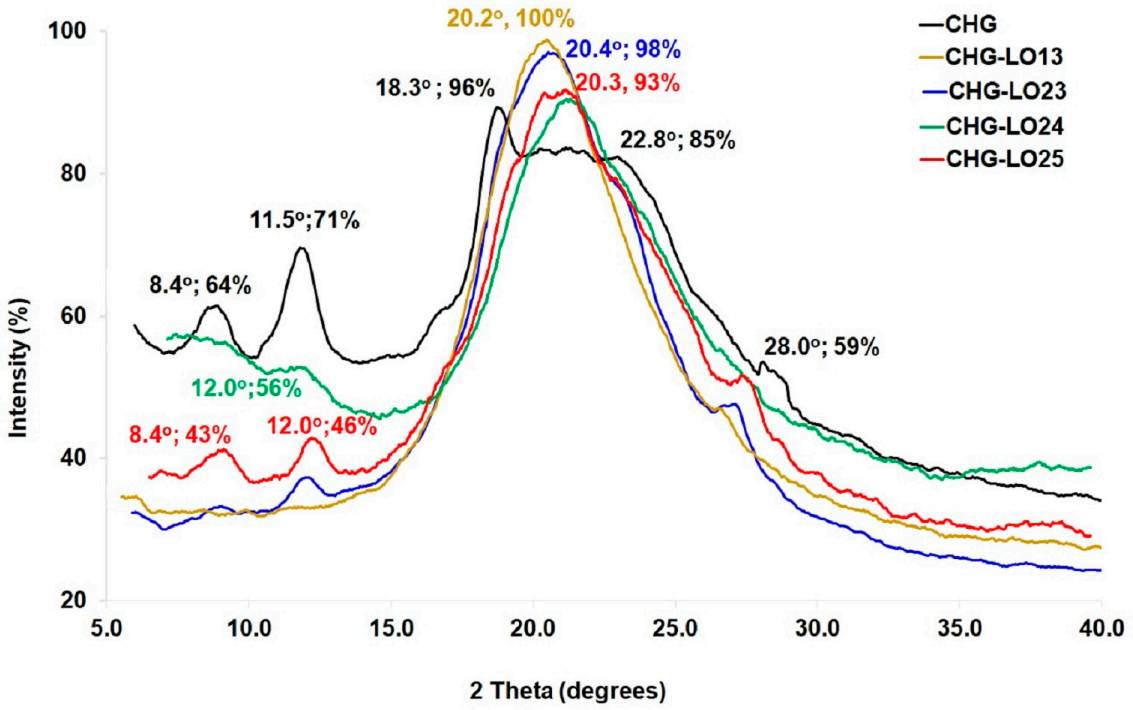

Figure 5. XRD graphs of CHG, CHG-LO13, CHG-LO23, CHG-LO24, and CHG-LO25 between 2θ of 5.00 and 40.00°.

3.2.3. The Surface Morphologies of the CHG Films

SEM images of the film samples are shown in Figure 6a–f. The SEM image of the CHG control film presents a smooth surface with no visible pores or cracks. EDS mapping of the control sample confirms the successful formation of a chitosan–gelatin network with thoroughly distributed calcium ions.

The surface morphologies of the CHG-LO films were influenced by the mass ratios of LO and OA within their structure; however, the formation of voids or cracks was not observed in their images. The SEM image of the film CHG–LO13 displayed a rough and fibrous surface, which can be attributed to the low ratio of LO (15 wt%) and high ratio of OA (38 wt%) in the film. The surfaces became more even and the rough and fibrous character of the surface morphology diminished in the film samples with higher LO ratios, CHG-LO23 (LO: 26 wt%; OA: 33 wt%) and CHG-LO24 (LO: 23 wt%; OA: 41 wt%), which is reminiscent of the effective surfactant behavior of OA during micelle formation, allowing a good dispersion of LO-OA in the film matrix. The surface of the sample CHG-LO25 (LO:21 wt%; OA: 47 wt%) exhibited a rougher surface with some wrinkle formations, likely due to the partial phase separation and agglomeration of LO-OA droplets near the surface, which coincides with the greater LO-OA concentration and the bigger particle size (see Z_{avg} values in Table 2). Vargas et al. pointed out that the increase in the OA content of the chitosan films leads to a considerable change in the surface topography, characterized by lipid particles on the surface [82]. Peng et al. reported that the incorporation of lemon essential oil increased the surface roughness of chitosan films and they observed more oil droplets in the SEM images of the films [83].

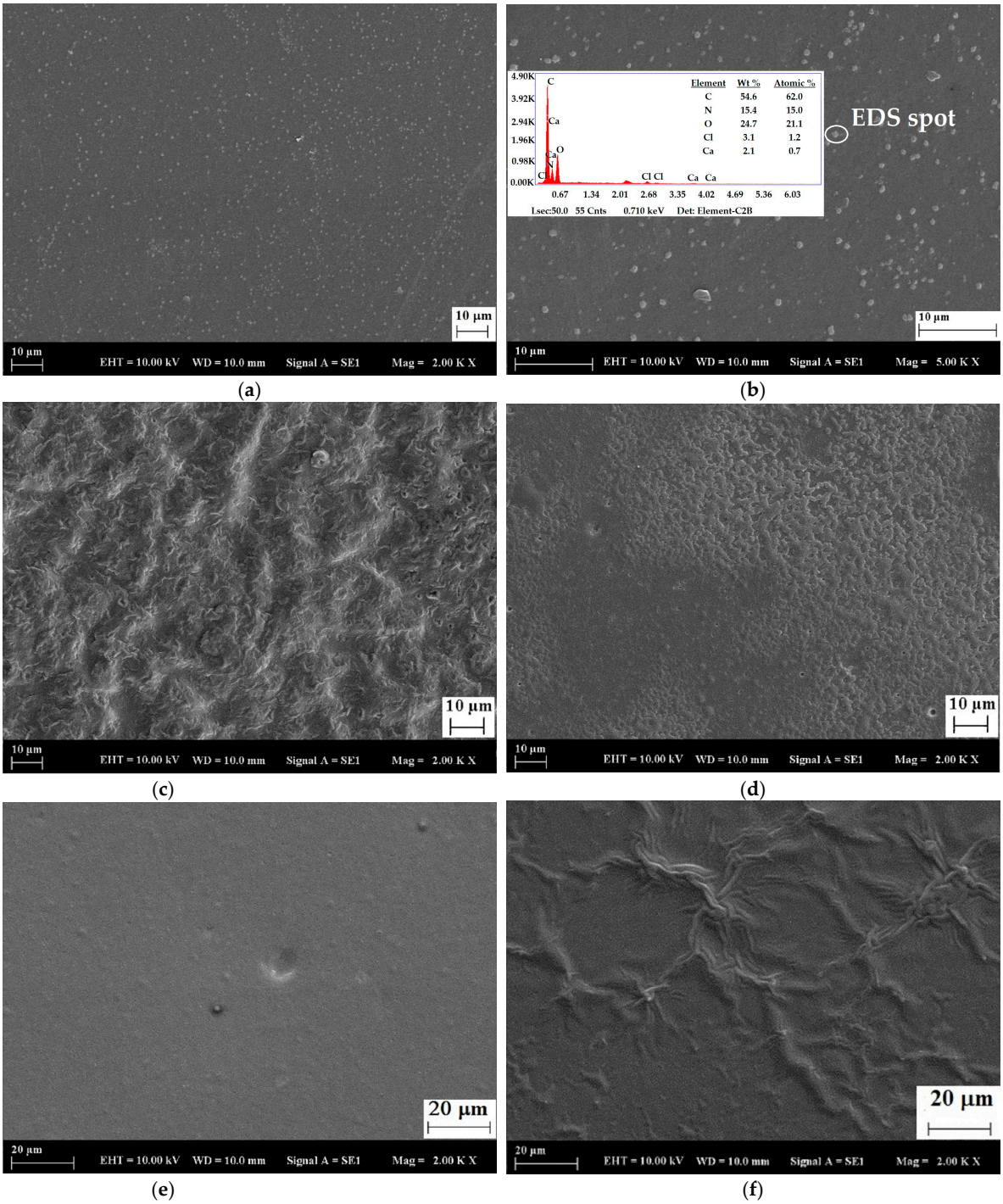

Figure 6. SEM images of: (**a**) CHG (×2000); (**b**) CHG (×5000) inlet: EDS spectrum of C, O, N, and Ca elements; (**c**) CHG–LO13 (×2000); (**d**) CHG–LO23 (×2000); (**e**) CHG–LO24 (×2000); (**f**) CHG–LO25 (×2000).

To gain further insight into the surface morphology of CHG-LO23, CHG-LO24, and CHG-LO25, these samples were subjected to additional analysis using Atomic Force Microscopy (AFM). Figure 7 displays the 2D and 3D AFM images of those films. The AFM results demonstrated that LO-OA droplets were dispersed throughout the film structures in agreement with the SEM images. In 2D AFM images of CHG-LO23, CHG-LO24, and CHG-LO25, the clustering of chitosan–gelatin chains around Ca^{2+} ions was observed as blackish dots on the surface. In addition, LO-OA droplets were distinguished as medium-dark and bright dots spread in the film structure [84].

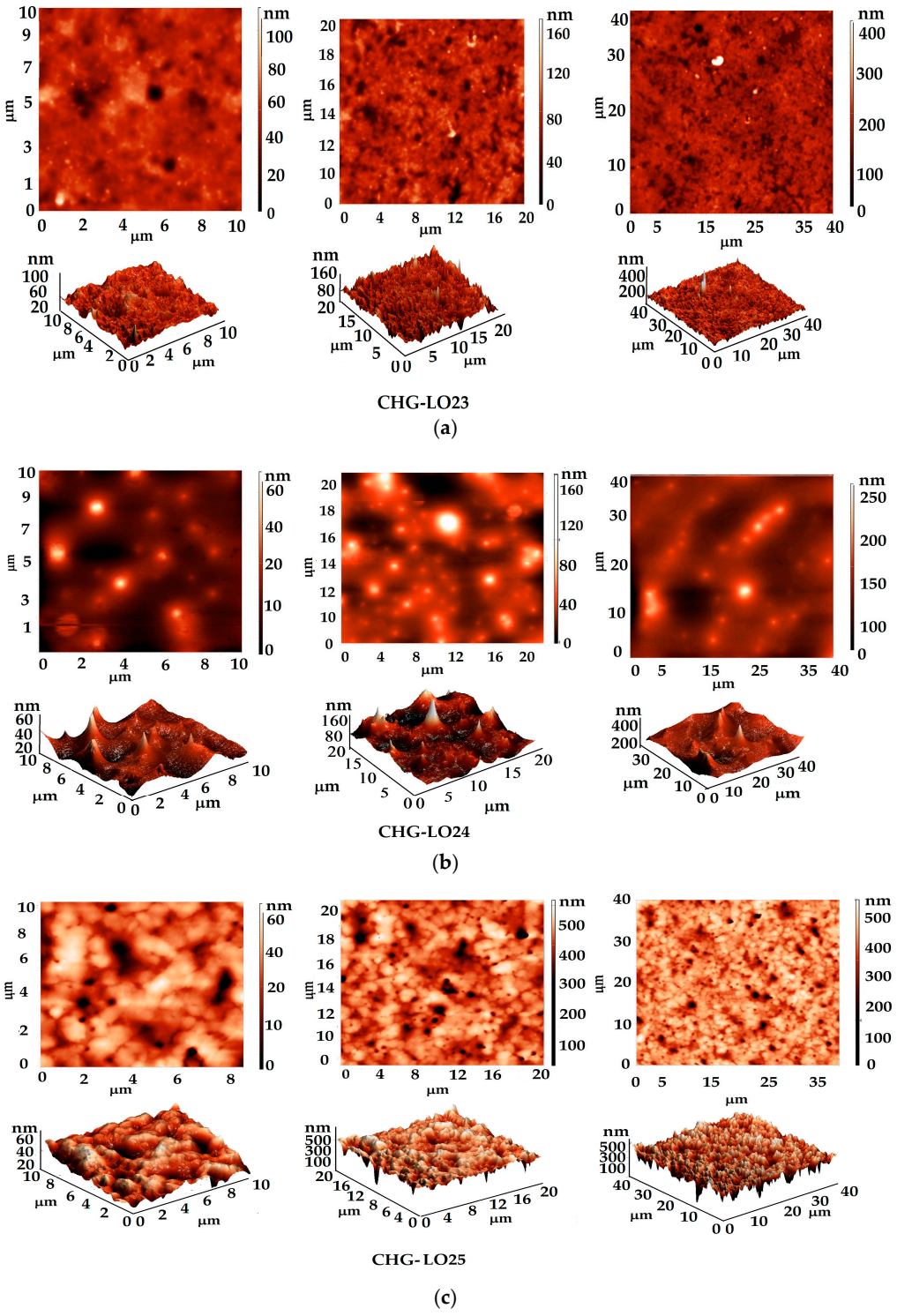

Figure 7. 2D and 3D AFM images of (**a**) CHG-LO23; (**b**) CHG-LO24, and (**c**) CHG-LO25 in a scanned area of 10, 20, and 40 μm^2.

Table 4 summarizes the quantitative surface parameters based on 3D AFM images for three different scan areas. The average surface roughness (Sa) and the root mean square roughness (Sq) values were significantly affected by the increase in the OA ratio in the films. The Sa values and Sq values of CHG-LO23 and CHG-LO24 film samples are very close to each other and lower than that of CHG-LO25. Concerning the ten-point average of the peak-to-valley heights (Sz), CHG-LO25 exhibits the highest values among all three samples. These results indicated smoother surfaces in CHG-LO23 and CHG-LO24 films

and higher surface roughness in the CHG-LO25 film, which can be attributed to the slight aggregation of increasing amounts of LO-OA micelles in the film matrix as seen in the SEM images obtained [85].

Table 4. Surface parameters of CHG-LO23, CHG-LO24, and CHG-LO25 films obtained from 3-D AFM images.

Parameter	CHG-LO23			CHG-LO24			CHG-LO25		
	10 µm	20 µm	40 µm	10 µm	20 µm	40 µm	10 µm	20 µm	40 µm
Ten-point average height, Sz (nm)	51.5	207.3	234.4	30.6	86.5	131.0	182.4	216.5	336.3
Average Roughness, Sa (nm)	9.2	13.5	13.0	4.7	11.4	16.4	29.8	35.7	41.7
Root Mean Square Roughness, Sq (nm)	11.6	23.5	21.2	6.6	15.9	23.7	38.8	49.0	60.1

3.2.4. Thermal Properties of CHG Films

Differential Scanning Calorimeter (DSC) Analysis Results of CHG Films

To evaluate the thermal energy storage properties of the films, DSC analyses were performed between −45–45 °C for ten heating-cooling cycles. Figure 8 illustrates the DSC thermograms of oleic acid and the samples CHG, CHG-LO20, CHG-LO13, CHG-LO23, CHG-LO24, and CHG-LO25. The detailed DSC results are given in Supporting Information S8. In DSC analyses, the phase change behavior of pure oleic acid was measured as 124.0 $J \cdot g^{-1}$ in the range of −29–17 °C during heating, indicating that OA is highly promising for food packaging applications as PCM. As can be seen in Figure 8b, the DSC curves of CHG control and CHG-LO20 (LO: 38 wt%, OA: 0 wt%) overlapped, showing no change in heat absorption or release behavior within the temperature range of −45 °C to 45 °C. On the other hand, during the heating cycle of DSC analysis, CHG-LO13, CHG-LO23, CHG-LO24, and CHG-LO25 film samples exhibited a significant increase in heat storage capacities to 14.0, 21.0, 29.0, and 36.0 $J \cdot g^{-1}$ in the temperature range from −26 °C to +20 °C, which coincides with the phase change behavior of OA. The heat storage efficiencies of these films were obtained as 30%, 51%, 57%, and 62%, respectively. In addition, they all maintained their high thermal energy storage capacity even after the 10th heating and cooling cycle and exhibited maximum heat absorption in the range of 1–7 °C (T_{peak}), making them suitable for thermal management in food packaging applications (see Figure 8b) [30].

Thermogravimetric (TG) Analysis Results of CHG Films

Results of thermogravimetric analyses of CHG films conducted in the temperature range of 25–600 °C are given in Figure 9. A three-step thermal decomposition was observed in all samples.

The thermal behavior of CHG control in the initial region was characterized by a 10% mass loss, during which the evaporation of residual water from the structure occurred at temperatures between 100 °C and 138 °C. The mass losses of the CHG film samples, which contained increasing amounts of LO and OA, remained at a level of 4–5% within the same temperature interval. This was attributed to the lower amount of water present in their structures [86].

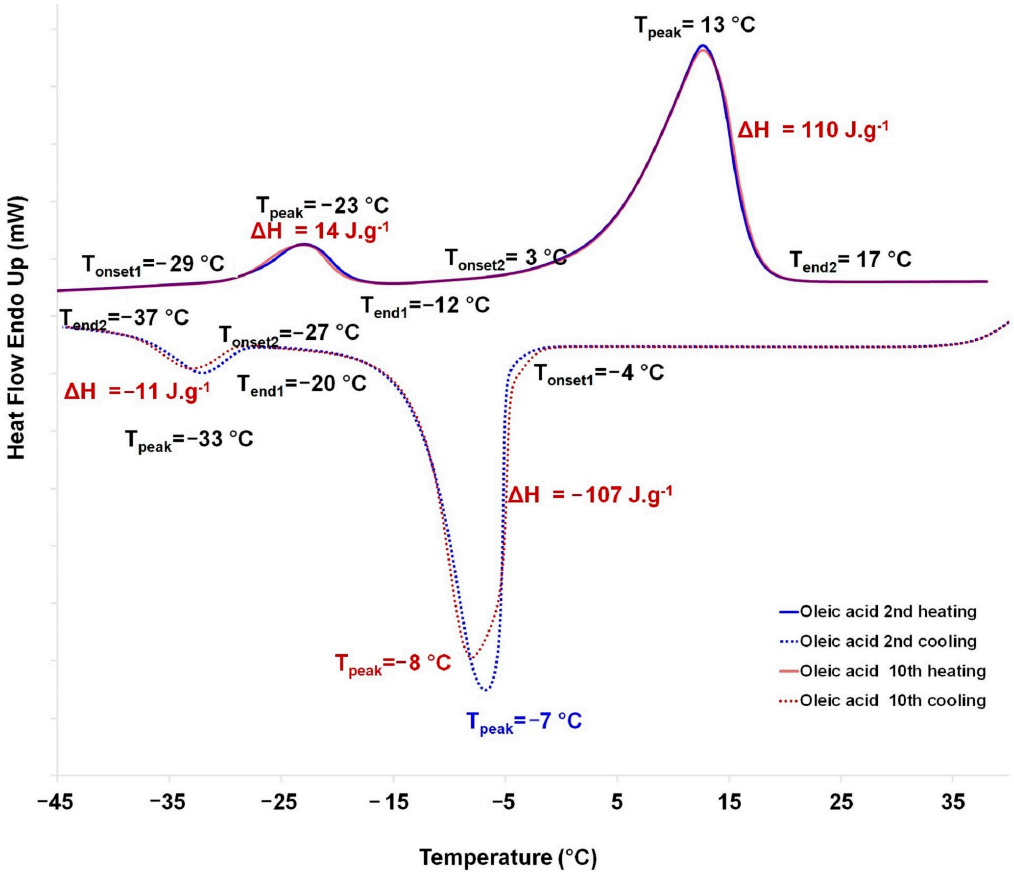

(**a**)

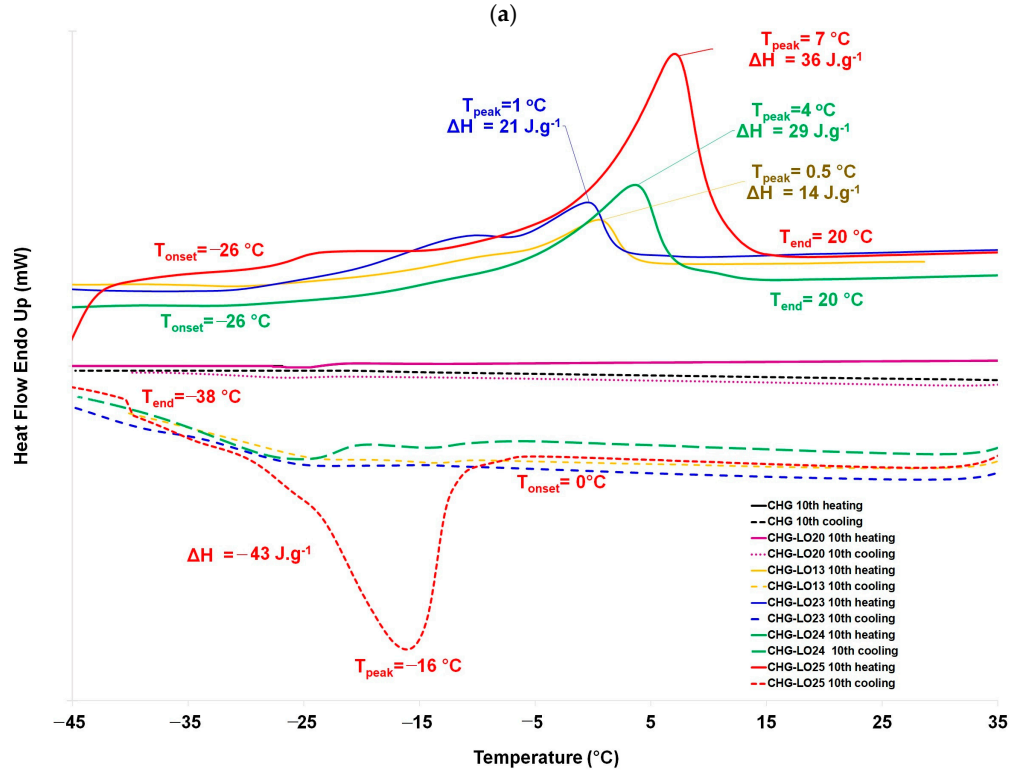

(**b**)

Figure 8. DSC curves obtained in the range of −45–35 °C at 10 °C.min^{-1}. (**a**) Pure oleic acid for the 2nd and 10th heating-cooling cycle; (**b**) CHG, CHG-LO20, CHG-LO13, CHG-LO23, CHG-LO24, and CHG-LO25 for the 10th heating-cooling cycle.

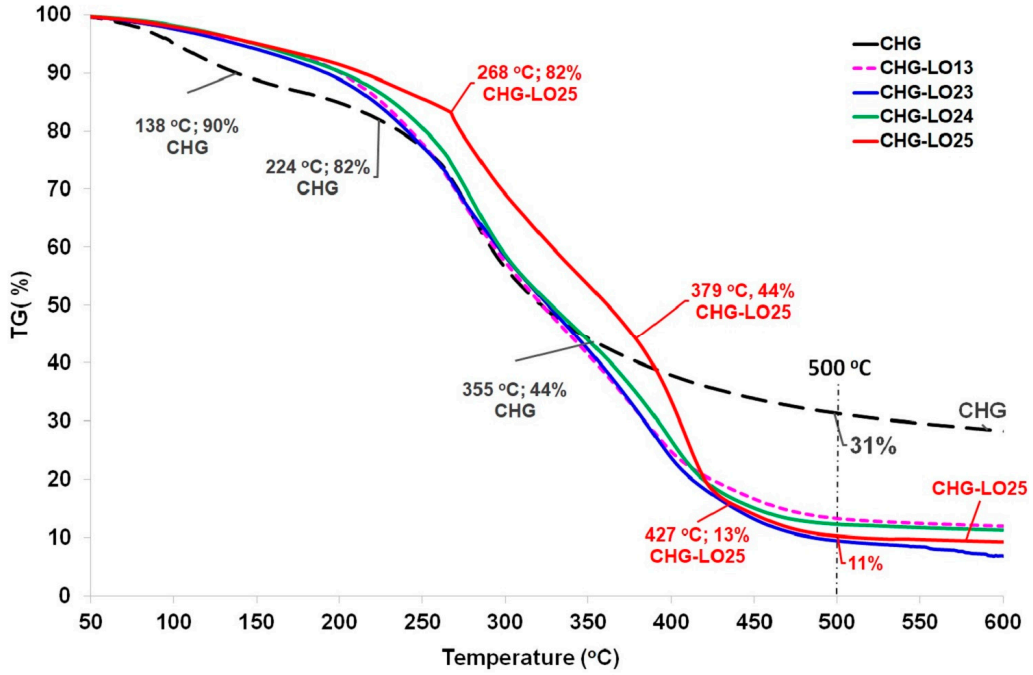

Figure 9. TG curves of CHG films.

In the second step, the mass losses of the CHG control and CHG-LO film samples accelerated from 222–268 °C and continued in a similar manner up to 355 °C, which was related to the thermal decomposition of chitosan and gelatin [33,87]. In the third step, the mass loss of the CHG control slowed down from 355 °C and the residual mass was 31% at 500 °C. On the other hand, the mass losses of CHG-LO films became faster from 355 °C to 450 °C due to the thermal decomposition of LO and OA in their structures, and the residual masses were about 11% at 500 °C. Similar initial and final temperatures and mass losses observed for the second step thermal degradation behavior of CHG-LO samples suggested that the incorporation of LO and OA did not impair the structural integrity of the chitosan–gelatin films [88].

3.2.5. pH-Dependent Swelling Degree, Water Solubility, and Water Vapor Transmission Rate (WVTR) Results of CHG Films

The swelling degree (S%) of the films in buffer solutions at pH = 3.0 and pH = 7.0 after 60 min, their water solubility (WS%) at the end of 24 h, and water vapor transmission rates (WVTR) of the CHG films are given in Table 5.

Table 5. Swelling degree (S%) (t = 60 min), water solubility (WS%) (t = 24 h), and water vapor transmission rates (WVTR) of CHG control and CHG-LO films.

Specimen	S (%)		WS (%)		WVTR ($g\ H_2O \cdot day^{-1} \cdot m^{-2}$)
	pH = 3.0	pH = 7.0	pH = 3.0	pH= 7.0	
CHG	71.4 ± 0.3	42.0 ± 0.4	58.2 ± 0.3	57.4 ± 0.3	568.4 ± 0.2
CHG–LO13	42.9 ± 0.2	37.2 ± 0.2	83.2 ± 0.3	78.4 ± 0.4	465.8 ± 0.2
CHG–LO20	36.8 ± 0.2	33.0 ± 0.1	87.2 ± 0.4	79.6 ± 0.3	437.1 ± 0.4
CHG–LO23	37.9 ± 0.3	30.9 ± 0.1	85.9 ± 0.1	81.1 ± 0.1	320.7 ± 0.3
CHG–LO24	45.0 ± 0.1	33.1 ± 0.3	88.1 ± 0.1	82.8 ± 0.3	416.2 ± 0.2
CHG–LO25	41.6 ± 0.1	28.9 ± 0.1	88.2 ± 0.2	84.3 ± 0.2	337.8 ± 0.1

The swelling degrees (S%) of all samples in an acidic medium were higher than in a neutral medium. The S% values of the CHG-LO films remained lower (37.9–44.9% at

pH 3.0 and 28.9–37.2% at pH 7.0) than those of the CHG control (71.4% at pH 3.0 and 42.0% at pH 7.0). This can be attributed to the presence of LO and OA, which limit the interactions between CHG chains and water molecules [89,90]. The S% of CHG-LO20 (LO: 38 wt%; OA: 0 wt%) also dropped to 36.8 at pH 3.0 and to 33.0 at pH 7.0, indicating that the presence of LO significantly affected and decreased the swelling degree of the CHG-LO20 film in the absence of OA. When CHG-LO13 (LO: 15 wt%; OA: 38 wt%) and CHG-LO23 (LO: 26 wt%; OA: 33 wt%) were compared with each other, the swelling tended to decrease due to the increase in the percentage of LO in the film structures. In the film samples CHG-LO24 (LO: 24 wt%; OA: 41 wt%) and CHG-LO25 (LO: 21 wt%; OA: 47 wt%), where OA ratios were the highest, the swelling degrees showed a slight increase compared to that of CHG-LO23 due to the increased interactions between the polar carboxylic acid (–COOH) ends of OA and water molecules. The decrease in swelling degrees was also reported in the study of Lian et al., who prepared chitosan–thyme essential oil composite films using four different surfactants, owing to the presence of essential oil [89]. A similar trend, i.e., a decrease in the swelling degree of chitosan films with EO content, was reported in the study of Sedlaříková et al., who modified chitosan with various concentrations of thyme essential oil and three types of surfactants with varying concentrations [90].

Although the addition of LO and OA significantly decreased the swelling degree, the water solubility (WS %) of CHG-LO films increased at both pH 3.0 and pH 7.0 within 24 h. The water solubility of the CHG-LO films was found to be significantly higher, reaching 79−88% at pH 3.0 and 67−84% at pH 7.0 compared to the solubility of the CHG control, which was 58.2% at pH 3.0 and 57.4% at pH 7.0. Lian et al. also found similar results in their study, explaining the increase of WS by the presence of increasing amounts of the surfactant causing essential oils to migrate from the chitosan film matrix to water [89]. As stated in the study of Sedlaříková et al., the increase in water solubility can be attributed to the increase in the hydrophilic groups included in phenolic compounds of LO and the carboxylic acid (-COOH) groups of OA, which resulted in interactions with water molecules [90].

Dang et al. stated that a decrease in water vapor permeability is an indication of the prevention of moisture transfer between the food and its surroundings, thereby extending the food's storage duration [91]. In the presence of LO-OA micelles, the WVTRs of CHG-LO films decreased by 18–44% compared to the CHG control owing to the increase of hydrophobic parts and hence improved their water barrier properties. These results are in agreement with the changes in their surface topographies observed in SEM and AFM images. Similar trends were reported in the studies of Vargas et al. [82] and Sedlaříková et al. [90].

3.2.6. The Contact Angle Measurement Results of the CHG Films

The contact angle measurement is a measure of the hydrophilic/hydrophobic behavior of film surfaces [91–93]. In general, a film surface with a contact angle $\theta w > 90^\circ$ is considered hydrophobic [94]. On the other hand, surfaces with water contact angles between $(56–65^\circ) < \theta w < 90^\circ$ are defined as weakly hydrophobic, and surfaces with water contact angles between $0^\circ < \theta w < (56–65^\circ)$ are defined as weakly hydrophilic [95].

Figure 10 illustrates the change in water contact angles (θw) of CHG films over time. The water contact angles of the samples declined slightly until 180 s, after which they remained more or less steady for the subsequent 120 s. The θ_W of the CHG control was 90.35° at t = 0 s and dropped to 80.92° at t = 180 s, demonstrating hydrophobic surface behavior. Even more, θ_W of the CHG-LO20 film, containing 38 wt% LO but no OA, reached 97.54° at t = 0 s and 92.70° at t = 180 s, exhibiting more hydrophobicity than the CHG control group [21,96,97], in parallel with the decrease in its swelling degree (see Section 3.2.5).

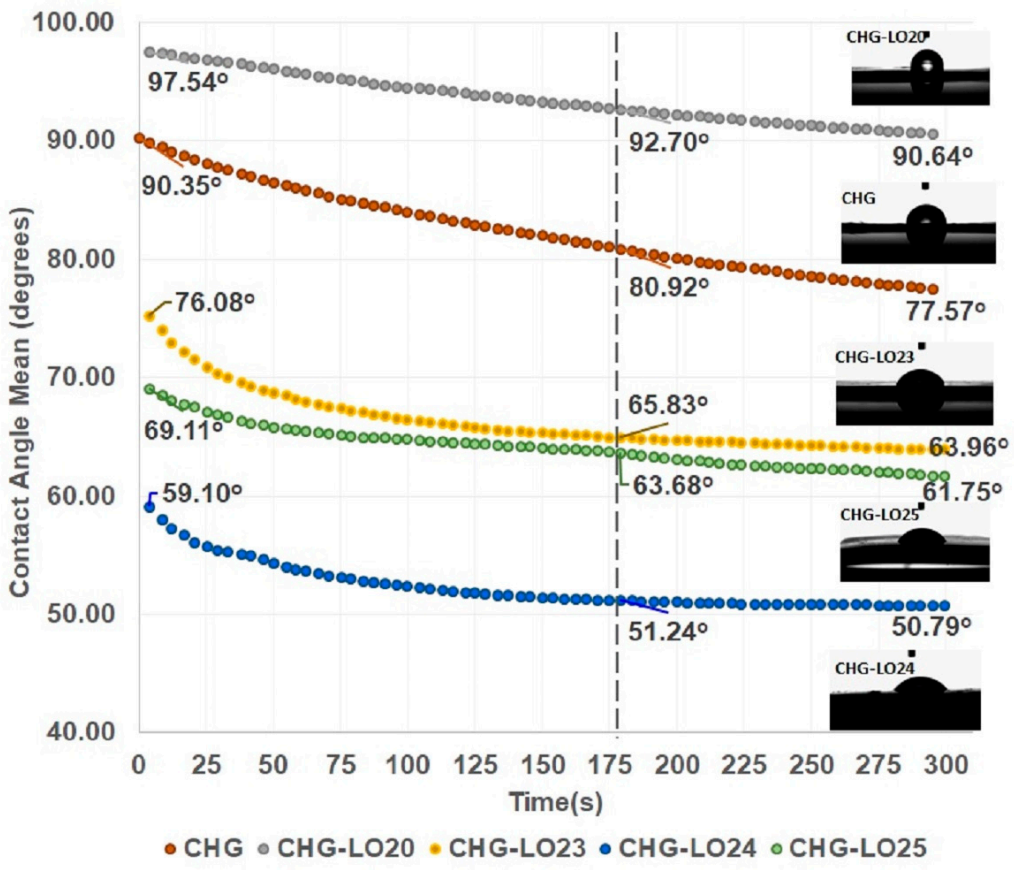

Figure 10. The change in the mean contact angle of CHG, CHG-LO20, CHG-LO23, CHG-LO24, and CHG-LO25 as a function of time, and the corresponding images of water droplets after 300 s.

The surface wettability properties of CHG-LO films were significantly influenced by the incorporation of OA in the presence of LO. A drop in contact angle occurred in all three cases when compared to CHG control and CHG-LO20. This result reveals that the addition of an increasing amount of OA, with its hydrophilic groups, can lead to increased interactions of the film surface with water, followed by a decrease in contact angle. These results are consistent with the observed slightly increasing trend in swelling degree caused by the presence of OA (see Section 3.2.5). However, the contact angles of all CHG-LO samples lie in the range of 59.10−76.08° at t = 0 s corresponding to the weak hydrophobic behavior. The higher contact angle value of CHG-LO25 compared to CHG-LO24 can be attributed to the increase in its surface roughness [98], which is consistent with the AFM results. The measured contact angles of the CHG-LO23, CHG-LO24, and CHG-LO25 samples maintained their weak hydrophobic surface behavior, with contact angles of 61.75° or above even at the 300th second [33,90,95].

3.2.7. Antioxidant and Antimicrobial Activity Results of CHG Films

Table 6 gives the results of the total phenolic content (TPC), DPPH (2,2-diphenyl-1-picrylhydrazyl) scavenging activity, and ABTS (2,2′–azino–bis(3–ethylbenzothiazoline–6–sulphonic acid) scavenging activity of the CHG films. The values obtained for the TPC in the LO-OA-containing film samples, increased 1.5–4.2 times compared to that of the CHG control, indicating improved antioxidant properties associated with the presence of lavender oil phenolic groups in the structure [99,100]. Similarly, the DPPH and ABTS scavenging activities showed an increase attributed to the bioactive and antioxidant components of lavender essential oil and oleic acid [101,102].

Table 6. Total phenolic content (TPC), DPPH, and ABTS free radical scavenging activities of CHG films.

Specimen	TPC [1] (GAE mg·g^{-1} Film)	DPPH Scavenging (%.g^{-1})	ABTS Scavenging [2] (TE µg·L^{-1}·g^{-1} Film)
CHG	2.48	5.70	30.2
CHG–LO13	6.75	12.1	32.0
CHG–LO23	7.62	12.3	35.6
CHG–LO24	6.51	7.90	39.8
CHG–LO25	6.90	7.10	40.5

[1] Gallic acid equivalent (GAE); [2] TROLOX equivalent (TE).

The antimicrobial activity results of the CHG films carried out according to four standard tests are summarized in Table 7. The common foodborne pathogens coliforms, coagulase-positive Staphylococci, Pseudomonas aeruginosa, and Listeria monocytogenes were not detected in any of the film samples according to the given standard test methods [61–64].

Table 7. Antimicrobial test results of CHG films.

Specimen	Coliforms Bacteria (kob/g)	Coagulase Positive Staphylococcus (kob/g)	Pseudomonas Aeruginosa (kob/g)	Listeria 1 Monocytogenes (kob/25 g)
CHG	<10 *	<100 **	<100 **	Not detected
CHG–LO13	<10 *	<100 **	<100 **	Not detected
CHG–LO23	<10 *	<100 **	<100 **	Not detected
CHG–LO24	<10 *	<100 **	<100 **	Not detected
CHG–LO25	<10 *	<100 **	<100 **	Not detected

* The uncertainty limit of the tests performed is <10 as specified in the standard; no bacterial growth was observed on the plate. ** The uncertainty limit of the tests performed is <100 as specified in the standard; no bacterial growth was observed on the plate.

4. Conclusions

In this study, we successfully developed bio-based chitosan–gelatin films containing different ratios of lavender essential oil (15–26 wt% LO) and oleic acid (33–47 wt% OA). The nanoemulsions were prepared first by ultrasonication to possess uniform dispersion and colloidal stability with average droplet sizes of 475–854 nm, polydispersity indices (PDI) of 0.095–0.235, and zeta potentials of 23.7–56.9 mV at 40 °C. Then CHG-LO films were successfully produced with smooth surfaces and thicknesses of 0.42–0.99 mm through the casting process.

The FTIR and XRD spectra confirm the structural integrity of chitosan, gelatin, LO, and OA within the CHG-LO films. According to the SEM images and AFM results, the surface morphologies of the CHG-LO films were influenced by the weight ratios of LO and OA. The surface morphologies of CHG-LO23 (LO: 26 wt%; OA: 33 wt%) and CHG-LO24 (LO: 23 wt%; OA: 41 wt%) became more even as evidence of the good dispersion of LO-OA in the film matrix. The opacities of all CHG-LO films increased by 1.8 to 5.5 times compared to the control group due to the light scattering induced by LO-OA droplets, and UV-visible light-blocking properties were improved which is critical for extending the shelf life of packaged products.

DSC analyses of CHG-LO13, CHG-LO23, CHG-LO24, and CHG-LO25 film samples exhibited a significant increase in heat storage capacities to 14.0, 21.0, 29.0, and 36.0 J·g^{-1} in the temperature range from −26 °C to +20 °C, which coincided with the phase change behavior of OA, so that the heat storage efficiencies were 30%, 51%, 57%, and 62%, respec-

tively. These thermal buffering capacities of the films, with maximum absorption enthalpies in the range of 1–7 °C, are promising to protect the food products from temperature changes where they are stored. According to TGA results, all CHG-LO samples were thermally stable up to 222–268 °C.

All CHG-LO samples showed reduced water vapor transmission rates by 18–44% compared to the control. Their swelling degrees in acidic and neutral environments were obtained as 37.9–44.9% and 28.9–37.2% in one hour, respectively, lower than those of the control; and their water solubility in 24 h reached 79–88% at pH 3.0 and 67–84% at pH 7.0. The CHG-LO23, CHG-LO24, and CHG-LO25 films indicate a weak hydrophobic surface character, with contact angles of 59.10–76.08° at t = 0 s. These results indicate their potential to minimize moisture exchange with the environment, thus contributing to the preservation of the freshness of packaged products.

The total phenolic contents of the CHG-LO films increased 1.5–4.2 times compared to the control associated with the presence of LO phenolic groups in the structure. DPPH and ABTS scavenging activity test results show that the antioxidant properties of these films improved with increasing LO-OA content up to 2.2 and 1.3 times the control, respectively, and also showed antimicrobial properties.

It has been concluded that the multifunctional CHG-LO films of this study, especially CHG-LO23, CHG-LO24, and CHG-LO25 are promising candidates for temperature-sensitive active packaging in the food industry due to their heat storage capacities along with their opacity in UV-visible regions, low surface wettability, good water vapor barrier, antioxidant, and antimicrobial properties. In a further study, after the production of CHG-LO films under industrial conditions, end-use tests such as packaging strength and durability, gas barrier properties, and both LO-OA migration and cytotoxicity when in contact with the food surface should also be performed. In addition, the thermal buffering behavior of these films should be tested, considering the various variable environmental conditions to which packaged foods are exposed.

5. Patents

Authors have patent application #A METHOD OF OBTAINING A PACKAGING FILM AND A PACKAGING FILM OBTAINED BY THE SAID METHOD (PCT/TR2023/050452) pending to be patented.

Supplementary Materials: The following supporting information can be downloaded at: https://www.mdpi.com/article/10.3390/polysaccharides6010017/s1, Table S1. The weight percentages of LO and OA, the total mass and thickness values of the CHG films; Table S2. DSC heating and cooling behavior of OA and the CHG films (10 °C.min^{-1}); Figure S1. FTIR spectrum of oleic acid (OA); Figure S2. FTIR spectrum of lavender oil (LO); Figure S3. FTIR spectrum of chitosan (CH); Figure S4. FTIR spectrum of gelatin (GE); Figure S5. FTIR spectrum of CHG control; Figure S6. FTIR spectrum of CHG−LO13; Figure S7. FTIR spectrum of CHG−LO23; Figure S8. FTIR spectrum of CHG−LO24; Figure S9. FTIR spectrum of CHG−LO25.

Author Contributions: Conceptualization, N.S. and E.O.; data curation, N.S. and E.O.; formal analysis, N.S. and E.O.; investigation, N.S., A.E. and E.O.; methodology, N.S., A.E. and E.O.; project administration, N.S.; resources, N.S.; validation, N.S., A.E. and E.O.; supervision, N.S.; visualization, N.S. and E.O.; writing—original draft, N.S. and E.O.; writing—review and editing, N.S. and E.O.; funding acquisition, N.S. All authors have read and agreed to the published version of the manuscript.

Funding: This work was based on the research project IKU BAP2102, which was funded by Istanbul Kultur University, 2021–2024.

Data Availability Statement: The original contributions presented in this study are included in the article. Further inquiries can be directed to the corresponding authors.

Acknowledgments: The authors would like to express their gratitude to Istanbul Kultur University for financial support in conducting this study.

Conflicts of Interest: The authors declare no conflicts of interest.

References

1. Market Research Future. *Food Packaging Market Research Report: Information by Material Type, Application, and by Region–Market Forecast Till 2032*; Market Research Future: Maharashtra, India, 2025. Available online: https://www.marketresearchfuture.com/reports/food-packaging-market-2086 (accessed on 10 January 2025).
2. Ahvenainen, R. (Ed.) Active and Intelligent Packaging: An Introduction. In *Novel Food Packaging Techniques*; Woodhead Publishing: Sawston, UK, 2003; pp. 5–21. [CrossRef]
3. European Commission. Regulation (EC) No 1935/2004 of the European Parliament and of the Council of 27 October 2004 on Materials and Articles Intended to Come into Contact with Food and Repealing Directives 80/590/EEC and 89/109/EEC. *Off. J. Eur. Union* **2004**, *L 338*, 4–17.
4. Dainelli, D.; Gontard, N.; Spyropoulos, D.; Zondervan-van den Beuken, E.; Tobback, P. Active and Intelligent Food Packaging: Legal Aspects and Safety Concerns. *Trends Food Sci. Technol.* **2008**, *19*, S103–S112. [CrossRef]
5. Dobrucka, R.; Przekop, R. New Perspectives in Active and Intelligent Food Packaging. *J. Food Process. Preserv.* **2019**, *43*, e14194. [CrossRef]
6. Ahmed, M.W.; Haque, M.A.; Mohibbullah, M.; Khan, M.S.I.; Islam, M.A.; Mondal, M.H.T.; Ahmmed, R. A Review on Active Packaging for Quality and Safety of Foods: Current Trends, Applications, Prospects, and Challenges. *Food Packag. Shelf Life* **2022**, *33*, 100913. [CrossRef]
7. Basavegowda, N.; Baek, K.H. Advances in Functional Biopolymer-Based Nanocomposites for Active Food Packaging Applications. *Polymers* **2021**, *13*, 4198. [CrossRef]
8. Shi, J.; Zhang, R.; Liu, X.; Zhang, Y.; Du, Y.; Dong, H.; Chen, F. Advances in Multifunctional Biomass-Derived Nanocomposite Films for Active and Sustainable Food Packaging. *Carbohydr. Polym.* **2023**, *301*, 120323. [CrossRef] [PubMed]
9. Ștefănescu, B.E.; Socaciu, C.; Vodnar, D.C. Recent Progress in Functional Edible Food Packaging Based on Gelatin and Chitosan. *Coatings* **2022**, *12*, 1815. [CrossRef]
10. Rathod, N.B.; Bangar, S.P.; Šimat, V.; Ozogul, F. Chitosan, and Gelatine Biopolymer-Based Active/Biodegradable Packaging for the Preservation of Fish and Fishery Products. *Int. J. Food Sci. Technol.* **2023**, *58*, 854–861. [CrossRef]
11. Wang, H.; Ding, F.; Ma, L.; Zhang, Y. Edible Films from Chitosan-Gelatin: Physical Properties and Food Packaging Application. *Food Biosci.* **2021**, *40*, 100871. [CrossRef]
12. Tyuftin, A.A.; Kerry, J.P. Gelatin Films: Study Review of Barrier Properties and Implications for Future Studies Employing Biopolymer Films. Food Packag. *Shelf Life* **2021**, *29*, 100688. [CrossRef]
13. Priyadarshi, R.; Rhim, J.W. Chitosan-Based Biodegradable Functional Films for Food Packaging Applications. *Innov. Food Sci. Emerg. Technol.* **2020**, *62*, 102346. [CrossRef]
14. Mittal, A.; Singh, A.; Benjakul, S.; Prodpran, T.; Nilsuwan, K.; Huda, N.; de la Caba, K. Composite Films Based on Chitosan and Epigallocatechin Gallate Grafted Chitosan: Characterization, Antioxidant and Antimicrobial Activities. *Food Hydrocoll.* **2021**, *111*, 106384. [CrossRef]
15. Hasan, M.; Rusman, R.; Khaldun, I.; Ardana, L.; Mudatsir, M.; Fansuri, H. Active Edible Sugar Palm Star-Chitosan Films Carrying Extra Virgin Olive Oil: Barrier, Thermo-Mechanical, Antioxidant, and Antimicrobial Properties. *Int. J. Biol. Macromol.* **2020**, *163*, 766–775. [CrossRef]
16. Al-Hashimi, A.G.; Ammar, A.B.; Cacciola, F.; Lakhssassi, N. Development of a Millet Starch Edible Film Containing Clove Essential Oil. *Foods* **2020**, *9*, 184. [CrossRef]
17. Cai, L.; Wang, Y.; Cao, A. The Physiochemical and Preservation Properties of Fish Sarcoplasmic Protein/Chitosan Composite Films Containing Ginger Essential Oil Emulsions. *J. Food Process Eng.* **2020**, *43*, e13495. [CrossRef]
18. Li, L.; Song, W.; Shen, C.; Dong, Q.; Wang, Y.; Zuo, S. Active Packaging Film Containing Oregano Essential Oil Microcapsules and Their Application for Strawberry Preservation. *J. Food Process Preserv.* **2020**, *44*, e14799. [CrossRef]
19. Firouz, M.S.; Mohi-Alden, K.; Omid, M. A Critical Review on Intelligent and Active Packaging in the Food Industry: Research and Development. *Food Res. Int.* **2021**, *141*, 110113. [CrossRef]
20. Jamróz, E.; Juszczak, L.; Kucharek, M. Investigation of the Physical Properties, Antioxidant and Antimicrobial Activity of Ternary Potato Starch-Furcellaran-Gelatin Films Incorporated with Lavender Essential Oil. *Int. J. Biol. Macromol.* **2018**, *114*, 1094–1101. [CrossRef]
21. Martucci, J.F.; Gende, L.B.; Neira, L.M.; Ruseckaite, R.A. Oregano, and Lavender Essential Oils as Antioxidant and Antimicrobial Additives of Biogenic Gelatin Films. *Ind. Crops Prod.* **2015**, *71*, 205–213. [CrossRef]

22. Hedayati, S.; Tarahi, M.; Iraji, A.; Hashempur, M.H. Recent Developments in the Encapsulation of Lavender Essential Oil. *Adv. Colloid. Interface Sci.* **2024**, *331*, 103229. [CrossRef]
23. U.S. Food and Drug Administration. Sec. 182.20 Essential Oils, Oleoresins (Solvent-Free), and Natural Extractives (Including Distillates). Title 21, Part 182.20. Available online: https://www.ecfr.gov/current/title-21/part-182/section-182.20 (accessed on 24 December 2024).
24. Prashar, A.; Locke, I.C.; Evans, C.S. Cytotoxicity of Lavender Oil and Its Major Components to Human Skin Cells. *Cell Prolif.* **2004**, *37*, 221–229. [CrossRef]
25. Llana-Ruiz-Cabello, M.; Pichardo, S.; Maisanaba, S.; Puerto, M.; Prieto, A.I.; Gutierrez-Praena, D.; Cameán, A.M. In Vitro Toxicological Evaluation of Essential Oils and Their Main Compounds Used in Active Food Packaging: A Review. *Food Chem. Toxicol.* **2015**, *81*, 9–27. [CrossRef]
26. Ribeiro-Santos, R.; Andrade, M.; de Melo, N.R.; Sanches-Silva, A. Use of Essential Oils in Active Food Packaging: Recent Advances and Future Trends. *Trends Food Sci. Technol.* **2017**, *61*, 132–140. [CrossRef]
27. Sun, X.; Wang, J.; Zhang, H.; Dong, M.; Li, L.; Jia, P.; Wang, L. Development of Functional Gelatin-Based Composite Films Incorporating Oil-in-Water Lavender Essential Oil Nano-Emulsions: Effects on Physicochemical Properties and Cherry Tomatoes Preservation. *LWT* **2021**, *142*, 110987. [CrossRef]
28. Gao, T.; Tian, Y.; Zhu, Z.; Sun, D.W. Modelling, Responses and Applications of Time-Temperature Indicators (TTIs) in Monitoring Fresh Food Quality. Trends Food Sci. *Technol.* **2020**, *99*, 311–322. [CrossRef]
29. Singh, S.; Lee, M.H.; Park, L.; Shin, Y.; Lee, Y.S. Antimicrobial Seafood Packaging: A Review. *J. Food Sci. Technol.* **2016**, *53*, 2505–2518. [CrossRef]
30. Singh, S.; Gaikwad, K.K.; Lee, M.; Lee, Y.S. Temperature-Regulating Materials for Advanced Food Packaging Applications: A Review. *Food Meas.* **2018**, *12*, 588–601. [CrossRef]
31. Gaikwad, K.K.; Singh, S.; Lee, Y.S. Oxygen Scavenging Films in Food Packaging. *Environ. Chem. Lett.* **2018**, *16*, 523–538. [CrossRef]
32. Feng, T.; Ji, J.; Zhang, X. Research Progress of Phase Change Cold Energy Storage Materials Used in Cold Chain Logistics of Aquatic Products. *J. Energy Storage* **2023**, *60*, 106568. [CrossRef]
33. Roy, S.; Min, S.J.; Rhim, J.W. Essential Oil-Added Chitosan/Gelatin-Based Active Packaging Film: A Comparative Study. *J. Compos. Sci.* **2023**, *7*, 126. [CrossRef]
34. Bahrami, S.; Sablani, S.S. Phase Change Materials in Food Packaging: A Review. *Food Bioprocess Technol.* **2024**, *1*, 1–24. [CrossRef]
35. Perez-Masia, R.; Lopez-Rubio, A.; Fabra, M.J.; Lagaron, J.M. Biodegradable Polyester-Based Heat Management Materials of Interest in Refrigeration and Smart Packaging Coatings. *J. Appl. Polym. Sci.* **2013**, *130*, 3251–3262. [CrossRef]
36. Pérez-Masiá, R.; López-Rubio, A.; Fabra, M.J.; Lagaron, J.M. Use of Electrohydrodynamic Processing to Develop Nanostructured Materials for the Preservation of the Cold Chain. *Innov. Food Sci. Emerg. Technol.* **2014**, *26*, 415–423. [CrossRef]
37. Chalco-Sandoval, W.; Fabra, M.J.; López-Rubio, A.; Lagaron, J.M. Development of Polystyrene-Based Films with Temperature Buffering Capacity for Smart Food Packaging. *J. Food Eng.* **2015**, *164*, 55–62. [CrossRef]
38. Tas, C.E.; Unal, H. Thermally Buffering Polyethylene/Halloysite/Phase Change Material Nanocomposite Packaging Films for Cold Storage of Foods. *J. Food Eng.* **2021**, *292*, 110351. [CrossRef]
39. Vahabi, F.; Bahrami, S.; Moslehishad, M. The Effect of Novel Packaging Containing Phase Change Material on Broccoli Quality During Storage. *Polymers* **2022**, *7*, 8.
40. Karim, M.; Fathi, M.; Soleimanian-Zad, S.; Spigno, G. Development of Sausage Packaging with Zein Nanofibers Containing Tetradecane Produced via Needle-Less Electrospinning Method. *Food Packag. Shelf Life* **2022**, *33*, 100911. [CrossRef]
41. U.S. Food and Drug Administration. *Oleic Acid. Title 21, Part 172.860.* Available online: https://www.ecfr.gov/current/title-21/part-172/section-172.860 (accessed on 26 December 2024).
42. Yuan, Y.; Zhang, N.; Tao, W.; Cao, X.; He, Y. Fatty Acids as Phase Change Materials: A Review. *Renew. Sustain. Energy Rev.* **2014**, *29*, 482–498. [CrossRef]
43. Nazari, M.; Jebrane, M.; Terziev, N. Multicomponent Bio-Based Fatty Acids System as Phase Change Material for Low Temperature Energy Storage. *J. Energy Storage* **2021**, *39*, 102645. [CrossRef]
44. Drago, E.; Campardelli, R.; Barbucci, A.; Perego, P. Polycaprolactone Sub-Micrometric Fibers Optimization for Primary Packaging Loaded with Fatty Acids as Natural Phase Change Materials. *J. Food Eng.* **2023**, *358*, 111680. [CrossRef]
45. Ghanbarzadeh, B.; Almasi, H. Physical Properties of Edible Emulsified Films Based on Carboxymethyl Cellulose and Oleic Acid. *Int. J. Biol. Macromol.* **2011**, *48*, 44–49. [CrossRef] [PubMed]
46. Khah, M.D.; Ghanbarzadeh, B.; Nezhad, L.R.; Ostadrahimi, A. Effects of Virgin Olive Oil and Grape Seed Oil on Physicochemical and Antimicrobial Properties of Pectin-Gelatin Blend Emulsified Films. *Int. J. Biol. Macromol.* **2021**, *171*, 262–274. [CrossRef]
47. Perdones, Á.; Chiralt, A.; Vargas, M. Properties of Film-Forming Dispersions and Films Based on Chitosan Containing Basil or Thyme Essential Oil. *Food Hydrocoll.* **2016**, *57*, 271–279. [CrossRef]
48. Ghasemlou, M.; Khodaiyan, F.; Oromiehie, A.; Yarmand, M.S. Characterization of Edible Emulsified Films with Low Affinity to Water Based on Kefiran and Oleic Acid. *Int. J. Biol. Macromol.* **2011**, *49*, 378–384. [CrossRef] [PubMed]

49. Ma, Q.; Hu, D.; Wang, H.; Wang, L. Tara Gum Edible Film Incorporated with Oleic Acid. *Food Hydrocoll.* **2016**, *56*, 127–133. [CrossRef]
50. Pinilla, C.M.B.; Thys, R.C.S.; Brandelli, A. Antifungal Properties of Phosphatidylcholine–Oleic Acid Liposomes Encapsulating Garlic Against Environmental Fungal in Wheat Bread. *Int. J. Food Microbiol.* **2019**, *293*, 72–78. [CrossRef]
51. Milano, F.; Masi, A.; Madaghiele, M.; Sannino, A.; Salvatore, L.; Gallo, N. Current Trends in Gelatin-Based Drug Delivery Systems. *Pharmaceutics* **2023**, *15*, 1499. [CrossRef]
52. Diass, K.; Merzouki, M.; Elfazazi, K.; Azzouzi, H.; Challioui, A.; Azzaoui, K.; Rhazi, L. Essential Oil of Lavandula officinalis: Chemical Composition and Antibacterial Activities. *Plants* **2023**, *12*, 1571. [CrossRef]
53. Roy, J.C.; Salaün, F.; Giraud, S.; Ferri, A.; Guan, J. Surface Behavior and Bulk Properties of Aqueous Chitosan and Type-B Gelatin Solutions for Effective Emulsion Formulation. *Carbohydr. Polym.* **2017**, *173*, 202–214. [CrossRef]
54. Bonilla, J.; Sobral, P.J. Investigation of the Physicochemical, Antimicrobial, and Antioxidant Properties of Gelatin-Chitosan Edible Film Mixed with Plant Ethanol-ic Extracts. *Food Biosci.* **2016**, *16*, 17–25. [CrossRef]
55. Gontard, N.; Duchez, C.; CUQ, J.L.; Guilbert, S. Edible Composite Films of Wheat Gluten and Lipids: Water Vapour Permeability and Other Physical Properties. *Int. J. Food Sci. Technol.* **1994**, *29*, 39–50. [CrossRef]
56. *ASTM E96-00e1*; Standard Test Methods for Water Vapor Transmission of Materials, Method. ASTM: Philadelphia, PA, USA, 2005.
57. Zhang, W.; Wahlgren, M.; Sivik, B. Membrane Characterization by the Contact Angle Technique: II. Characterization of UF-Membranes and Comparison between the Captive Bubble and Sessile Drop as Methods to Obtain Water Contact Angles. *Desalination* **1989**, *72*, 263–273. [CrossRef]
58. Tessaro, L.; Luciano, C.G.; Bittante, A.M.Q.B.; Lourenço, R.V.; Martelli-Tosi, M.; do Amaral Sobral, P.J. Gelatin and/or Chitosan-Based Films Activated with "Pitanga" (*Eugenia uniflora* L.) Leaf Hydroethanolic Extract Encapsulated in Double Emulsion. *Food Hydrocoll.* **2021**, *113*, 106523. [CrossRef]
59. Mehdizadeh, T.; Tajik, H.; Razavi Rohani, S.M.; Oromiehie, A.R. Antibacterial, Antioxidant, and Optical Properties of Edible Starch-Chitosan Composite Film Containing Thymus kotschyanus Essential Oil. *Vet. Res. Forum* **2012**, *3*, 167–173.
60. Re, R.; Pellegrini, N.; Proteggente, A.; Pannala, A.; Yang, M.; Rice-Evans, C. Anti-oxidant Activity Applying an Improved ABTS Radical Cation Decolorization Assay. *Free Radic. Biol. Med.* **1999**, *26*, 1231–1237. [CrossRef]
61. *ISO 4832:2006*; Microbiology of Food and Animal Feeding Stuffs—Horizontal Method for the Enumeration of Coli-Forms—Colony-Count Technique. International Organization for Standardization: Geneva, Switzerland, 2021. Available online: https://www.iso.org/standard/38282.html (accessed on 24 October 2024).
62. *ISO 6888-1:2021*; Microbiology of the Food Chain—Horizontal Method for the Enumeration of Coagulase-Positive Staphylococci (Staphylococcus aureus and Other Species) Part 1: Method Using Baird-Parker Agar Medium. International Organization for Standardization: Geneva, Switzerland, 2021. Available online: https://www.iso.org/standard/76672.html (accessed on 24 October 2024).
63. *ISO 13720:2010*; Meat and Meat Products—Enumeration of Presumptive *Pseudomonas* spp. International Organization for Standardization: Geneva, Switzerland, 2010. Available online: https://www.iso.org/standard/45099.html (accessed on 24 October 2024).
64. *ISO 11290-1:2017*; Microbiology of the Food Chain—Horizontal Method for the Detection and Enumeration of Listeria monocytogenes and of *Listeria* spp. Part 1: Detection Method. International Organization for Standardization: Geneva, Switzerland, 2017. Available online: https://www.iso.org/standard/60313.html (accessed on 24 October 2024).
65. Melro, E.; Antunes, F.E.; da Silva, G.J.; Cruz, I.; Ramos, P.E.; Carvalho, F.; Alves, L. Chitosan Films in Food Applications: Tuning Film Properties by Changing Acidic Dissolution Conditions. *Polymers* **2020**, *13*, 1. [CrossRef] [PubMed]
66. Detsi, A.; Kavetsou, E.; Kostopoulou, I.; Pitterou, I.; Pontillo, A.R.N.; Tzani, A.; Zoumpoulakis, P. Nanosystems for the Encapsulation of Natural Products: The Case of Chitosan Biopolymer as a Matrix. *Pharmaceutics* **2020**, *12*, 669. [CrossRef]
67. Xavier, L.O.; Sganzerla, W.G.; Rosa, G.B.; da Rosa, C.G.; Agostinetto, L.; de Lima Veeck, A.P.; Nunes, M.R. Chitosan Packaging Functionalized with Cinnamodendron dinisii Essential Oil Loaded Zein: A Proposal for Meat Conservation. *Int. J. Biol. Macromol.* **2021**, *169*, 183–193. [CrossRef]
68. Sharma, N.; Kaur, G.; Khatkar, S.K. Optimization of Emulsification Conditions for Designing Ultrasound Assisted Curcumin Loaded Nanoemulsion: Characterization, Antioxidant Assay and Release Kinetics. *LWT* **2021**, *141*, 110962. [CrossRef]
69. Sánchez-González, L.; Chiralt, A.; González-Martínez, C.; Cháfer, M. Effect of Essential Oils on Properties of Film Forming Emulsions and Films Based on Hydroxypropylmethylcellulose and Chitosan. *J. Food Eng.* **2011**, *105*, 246–253. [CrossRef]
70. Moalla, S.; Ammar, I.; Fauconnier, M.L.; Danthine, S.; Blecker, C.; Besbes, S.; Attia, H. Development and Characterization of Chitosan Films Carrying Artemisia campestris Antioxidants for Potential Use as Active Food Packaging Materials. *Int. J. Biol. Macromol.* **2021**, *183*, 254–266. [CrossRef] [PubMed]
71. Lei, Y.; Mao, L.; Yao, J.; Zhu, H. Improved Mechanical, Antibacterial and UV Barrier Properties of Catechol-Functionalized Chitosan/Polyvinyl Alcohol Biodegradable Composites for Active Food Packaging. *Carbohydr. Polym.* **2021**, *264*, 117997. [CrossRef] [PubMed]

72. Nguyen, T.T.; Nguyen, T.T.T.; Tran, T.V.; Tan, L.V.; Danh, L.T.; Than, V.T. Development of Antibacterial, Antioxidant, and UV-Barrier Chitosan Film Incorporated with Piperbetle Linn Oil as Active Biodegradable Packaging Material. *Coatings* **2021**, *11*, 351. [CrossRef]
73. Carvalho, I.C.; Mansur, H.S. Engineered 3D-Scaffolds of Photocrosslinked Chitosan-Gelatin Hydrogel Hybrids for Chronic Wound Dressings and Regeneration. *Mater. Sci. Eng. C* **2017**, *78*, 690–705. [CrossRef]
74. Hosseini, S.F.; Rezaei, M.; Zandi, M.; Farahmandghavi, F. Development of Bioactive Fish Gelatin/Chitosan Nanoparticles Composite Films with Antimicrobial Properties. *Food Chem.* **2016**, *194*, 1266–1274. [CrossRef]
75. López-Mata, M.A.; Ruiz-Cruz, S.; Silva-Beltrán, N.P.; Ornelas-Paz, J.D.J.; Zamudio-Flores, P.B.; Burruel-Ibarra, S.E. Physicochemical, Antimicrobial and Antioxidant Properties of Chitosan Films Incorporated with Carvacrol. *Molecules* **2013**, *18*, 13735–13753. [CrossRef]
76. Tarhan, İ.; Çelikten, Ş.; Kestek, H.M.; Çelik, B.; Öner, M.; Kenar, A.; Kara, H. Development of a New and Rapid FTIR Method Using Chemometric Modeling Techniques for the Determination of Lavandin Adulteration in Lavender Essential Oil. *Vibr. Spectrosc.* **2023**, *127*, 103559. [CrossRef]
77. Sirvaityte, J.; Siugzdaite, J.; Valeika, V. Application of Commercial Essential Oils of Eucalyptus and Lavender as Natural Preservative for Leather Tanning Industry. *Rev. Chim.* **2011**, *62*, 884–893.
78. Lee, D.H.; Condrate Sr, R.A. FTIR Spectral Characterization of Thin Film Coatings of Oleic Acid on Glasses: I. Coatings on Glasses from Ethyl Alcohol. *J. Mater. Sci.* **1999**, *34*, 139–146. [CrossRef]
79. Valencia, G.A.; Lourenço, R.V.; Bittante, A.M.Q.B.; do Amaral Sobral, P.J. Physical and Morphological Properties of Nanocomposite Films Based on Gelatin and Laponite. *Appl. Clay Sci.* **2016**, *124*, 260–266. [CrossRef]
80. Pérez-Córdoba, L.J.; Norton, I.T.; Batchelor, H.K.; Gkatzionis, K.; Spyropoulos, F.; Sobral, P.J. Physico-Chemical, Antimicrobial and Antioxidant Properties of Gelatin-Chitosan Based Films Loaded with Nanoemulsions Encapsulating Active Compounds. *Food Hydrocoll.* **2018**, *79*, 544–559. [CrossRef]
81. Rubilar, J.F.; Cruz, R.M.; Silva, H.D.; Vicente, A.A.; Khmelinskii, I.; Vieira, M.C. Physico-Mechanical Properties of Chitosan Films with Carvacrol and Grape Seed Extract. *J. Food Eng.* **2013**, *115*, 466–474. [CrossRef]
82. Vargas, M.; Albors, A.; Chiralt, A.; González-Martínez, C. Characterization of Chitosan–Oleic Acid Composite Films. *Food Hydrocoll.* **2009**, *23*, 536–547. [CrossRef]
83. Peng, Y.; Yin, L.; Li, Y. Combined Effects of Lemon Essential Oil and Surfactants on Physical and Structural Properties of Chitosan Films. *Int. J. Food Sci. Technol.* **2013**, *48*, 44–50. [CrossRef]
84. Jahed, E.; Khaledabad, M.A.; Almasi, H.; Hasanzadeh, R. Physicochemical Properties of Carum copticum Essential Oil Loaded Chitosan Films Containing Organic Nano Reinforcements. *Carbohydr. Polym.* **2017**, *164*, 325–338. [CrossRef]
85. Ma, W.; Tang, C.H.; Yin, S.W.; Yang, X.Q.; Wang, Q.; Liu, F.; Wei, Z.H. Characterization of Gelatin-Based Edible Films Incorporated with Olive Oil. *Food Res. Int.* **2012**, *49*, 572–579. [CrossRef]
86. Shen, Z.; Kamdem, D.P. Development and Characterization of Biodegradable Chitosan Films Containing Two Essential Oils. *Int. J. Biol. Macromol.* **2015**, *74*, 289–296. [CrossRef]
87. Qiao, C.; Ma, X.; Zhang, J.; Yao, J. Molecular Interactions in Gelatin/Chitosan Composite Films. *Food Chem.* **2017**, *235*, 45–50. [CrossRef] [PubMed]
88. Dong, Z.; Xu, F.; Ahmed, I.; Li, Z.; Lin, H. Characterization and Preservation Performance of Active Polyethylene Films Containing Rosemary and Cinnamon Essential Oils for Pacific White Shrimp Packaging. *Food Control* **2018**, *92*, 37–46. [CrossRef]
89. Lian, H.; Peng, Y.; Shi, J.; Wang, Q. Effect of Emulsifier Hydrophilic-Lipophilic Balance (HLB) on the Release of Thyme Essential Oil from Chitosan Films. *Food Hydrocoll.* **2019**, *97*, 105213. [CrossRef]
90. Sedlaříková, J.; Janalíková, M.; Rudolf, O.; Pavlačková, J.; Egner, P.; Peer, P.; Krejčí, J. Chitosan/Thyme Oil Systems as Affected by Stabilizing Agent: Physical and Anti-microbial Properties. *Coatings* **2019**, *9*, 165. [CrossRef]
91. Dang, X.; Han, S.; Du, Y.; Fei, Y.; Guo, B.; Wang, X. Engineered Environment-Friendly Multifunctional Food Packaging with Superior Nonleachability, Polymer Miscibility, and Antimicrobial Activity. *Food Chem.* **2025**, *466*, 142192. [CrossRef]
92. Pereda, M.; Amica, G.; Marcovich, N.E. Development and Characterization of Edible Chitosan/Olive Oil Emulsion Films. *Carbohydr. Polym.* **2012**, *87*, 1318–1325. [CrossRef]
93. Sahraee, S.; Milani, J.M.; Ghanbarzadeh, B.; Hamishehkar, H. Effect of Corn Oil on Physical, Thermal, and Antifungal Properties of Gelatin-Based Nanocomposite Films Containing Nano Chitin. *LWT—Food Sci. Technol.* **2017**, *76*, 33–39. [CrossRef]
94. Dong, Y.; Rao, Z.; Liu, Y.; Zheng, X.; Tang, K.; Liu, J. Soluble Soybean Polysaccharide/Gelatin Active Edible Films Incorporated with Curcumin for Oil Packaging. *Food Packag. Shelf Life* **2023**, *35*, 101039. [CrossRef]
95. Drelich, J.; Chibowski, E.; Meng, D.D.; Terpilowski, K. Hydrophilic and Superhydrophilic Surfaces and Materials. *Soft Matter* **2011**, *7*, 9804–9828. [CrossRef]
96. Ojagh, S.M.; Rezaei, M.; Razavi, S.H.; Hosseini, S.M.H. Development and Evaluation of a Novel Biodegradable Film Made from Chitosan and Cinnamon Essential Oil with Low-Affinity Toward Water. *Food Chem.* **2010**, *122*, 161–166. [CrossRef]

97. Scartazzini, L.; Tosati, J.V.; Cortez, D.H.C.; Rossi, M.J.; Flôres, S.H.; Hubinger, M.D.; Monteiro, A.R. Gelatin Edible Coatings with Mint Essential Oil (*Mentha arvensis*): Film Characterization and Antifungal Properties. *J. Food Sci. Technol.* **2019**, *56*, 4045–4056. [CrossRef]
98. Wenzel, R.N. Resistance of Solid Surfaces to Wetting by Water. *Ind. Eng. Chem.* **1936**, *28*, 988–994. [CrossRef]
99. Xie, W.; Xu, P.; Liu, Q. Antioxidant Activity of Water-Soluble Chitosan Derivatives. *Bioorg. Med. Chem. Lett.* **2001**, *11*, 1699–1701. [CrossRef]
100. Kchaou, H.; Benbettaïeb, N.; Jridi, M.; Abdelhedi, O.; Karbowiak, T.; Brachais, C.H.; Nasri, M. Enhancement of Structural, Functional and Antioxidant Properties of Fish Gelatin Films Using Maillard Reactions. *Food Hydrocoll.* **2018**, *83*, 326–339. [CrossRef]
101. Danh, L.T.; Triet, N.D.A.; Zhao, J.; Mammucari, R.; Foster, N. Antioxidant Activity, Yield and Chemical Composition of Lavender Essential Oil Extracted by Supercritical CO_2. *J. Supercrit. Fluids* **2012**, *70*, 27–34. [CrossRef]
102. García, A.V.; Álvarez-Pérez, O.B.; Rojas, R.; Aguilar, C.N.; Garrigós, M.C. Impact of Olive Extract Addition on Corn Starch-Based Active Edible Films Properties for Food Packaging Applications. *Foods* **2020**, *9*, 1339. [CrossRef] [PubMed]